NASA CONTRACTOR

REPORT

NASA CR – 132460

SUBSTANTIATION DATA FOR

ADVANCED BEADED AND TUBULAR STRUCTURAL PANELS

Volume 1, DESIGN AND ANALYSIS

By
Bruce E. Greene

THE BOEING COMPANY

Prepared For
NATIONAL AERONAUTICS AND SPACE ADMINISTRATION

NASA Langley Research Center
Contract NAS1-10749
John L. Shideler Project Manager

NASA CR – 132460

SUBSTANTIATION DATA FOR

ADVANCED BEADED AND TUBULAR STRUCTURAL PANELS

Volume 1, DESIGN AND ANALYSIS

By
Bruce E. Greene

THE BOEING COMPANY

Prepared For
NATIONAL AERONAUTICS AND SPACE ADMINISTRATION

NASA Langley Research Center
Contract NAS1-10749

FOREWORD

This report was prepared by The Boeing Aerospace Company, a division of The Boeing Company, Seattle, Washington for the Langley Research Center of the National Aeronautics and Space Administration. The strength analysis, design, and correlation with tests of advanced beaded and tubular structural panel specimens is presented. The work is part of a comprehensive program to develop advanced beaded and tubular structural panel designs and static strength prediction methods under contract NASI-10749, "Design and Testing of Advanced Structural Panels." This program was under the cognizance of Herman L. Bohon and John L. Shideler of the Thermal Protection Section of the Structures and Dynamics Division, Langley Research Center.

The principal investigator on this program was Bruce E. Greene. The technical leader was Max D. Musgrove, reporting to the program manager, John L. Arnquist, Chief of the Structural Methods and Allowables organization.

This report was prepared by Bruce E. Greene in cooperation with John L. Shideler.

The art work and drafts for this report were prepared by Gary Jensen.

Abstract

A study was conducted to exploit the efficiency of curved elements in the design of lightweight structural panels under combined loads of axial compression, inplane shear, and bending. A summary of the total program (analysis, fabrication and test) is presented in document NASA CR-2514. The report presented herein is a supplement to the summary document and contains detailed analytical procedures for optimum panel design, static strength analyses, results of panel design studies, and correlation of theory with test results. Detailed descriptions of the fabrication development and of the panel tests are contained in supplementary documents NASA CR-132482, and NASA CR-132515, respectively.

The work reported herein has resulted in a verified analysis and design procedure for one of the panel configurations studied. Typical design curves for this configuration are presented. Comparison of test results with theory for the other three configurations shows poor agreement, and a verified design procedure for these concepts was not attained. The need for further analytical effort is discussed.

CONTENTS

		Page
NOMENCLATURE		viii
SUMMARY		1
INTRODUCTION		2
11.0*	DESIGN AND ANALYSIS PROCEDURES	4
11.1	Optimum Design (OPTRAN)	4
11.2	Strength Predictions (PANAP)	5
12.0	STATIC STRENGTH ANALYSIS	6
12.1	Section Properties	6
12.2	Stress Analysis	17
12.3	Failure Mode Analysis	19
12.4	Compression - Shear Interaction	24
12.5	Plasticity Corrections	25
13.0	PANEL DESIGN STUDIES	34
13.1	Initial Trade Studies	34
13.2	Final Design Selections	39
14.0	CORRELATION WITH TEST DATA	44
14.1	Correlation of Panel Type 2 Data	46
14.1.1	Local Buckling Specimen Test Data	46
14.1.2	Panel Test Data	50
14.2	Correlation of Panel Type 1A Data	54
14.2.1	Local Buckling Specimen Test Data	54
14.2.2	Panel Test Data	54
14.3	Correlation of Panel Type 2A-1 Data	60
14.3.1	Local Buckling Specimen Test Data	60
14.3.2	Panel Test Data	60
14.4	Correlation of Panel Type 2A-2 Data	66
14.4.1	Local Buckling Specimen Test Data	66
14.4.2	Panel Test Data	69
15.0	RESULTS AND CONCLUSIONS	74
REFERENCES		78

* Section numbers have been assigned to provide separate section numbers throughout the three substantiating data documents.

LIST OF FIGURES

No.	Title	Page
12-1	Basic Geometry of Beaded and Tubular Panel Configurations	8
12-2	Detailed Geometries of Single-Sheet Configurations for Calculation of Section Properties	9
12-3	Buckling of Cylindrical Sheets Subject to Axial Compression and Bending	22
12-4	Plasticity Correction Curves	27
12-5	Plasticity Corrections to Combined Load Failure Analysis	28
13-1	Weight Penalty Vs. Bead Angle and Flat Width-Panel Type 1	35
13-2	Weight Penalty Vs. Flat Width, Various Load Levels-Panel Type 1	37
13-3	Weight Penalty Vs. Bead Angle for Various Loads-Panel Type 2	38
13-4	Comparative Weights of Beaded and Tubular Panel Configurations	40
13-5	Optimum Panel Designs Selected for Final Development	41
13-6	Optimum Panel Designs as Manufactured with Revised Strength Predictions	43
14-1	Correlation of Local Buckling Test Results with Analysis-Panel Type 2	47
14-2	Local Buckling Test/Analysis Correlation-Panel Type 2	48
14-3	Correlation of Local Buckling Test Results with Analysis-Panel Type 1A	51
14-4	Local Buckling Test/Analysis Correlation-Panel Type 1A	52
14-5	Correlation of Local Buckling Test Results with Analysis-Panel Type 2A-1	55
14-6	Local Buckling Test/Analysis Correlation-Panel Type 2A-1	56
14-7	Correlation of Local Buckling Test Results with Analysis-Panel Type 2A-2	58
14-8	Local Buckling Test/Analysis Correlation-Panel Type 2A-2	59
14-9	Final Test/Analysis Correlation Summary-Panel Type 2	61

LIST OF FIGURES (Continued)

No.	Title	Page
14-10	Theoretical Failure Load Interaction Surface Showing Correlation with Test Data-Panel Type 2	62
14-11	Final Test/Analysis Correlation Summary-Panel Type 1A	64
14-12	Theoretical Failure Load Interaction Surface Showing Correlation with Test Data-Panel Type 1A	65
14-13	Final Test/Analysis Correlation Summary-Panel Type 2A-1	67
14-14	Theoretical Failure Load Interaction Surface Showing Correlation with Test Data-Panel Type 2A-1	68
14-15	Final Test/Analysis Correlation Summary-Panel Type 2A-2	70
14-16	Theoretical Failure Load Interaction Surface Showing Correlation with Test Data-Panel Type 2A-2	71
15-1	Tubular Panel Design Data	75

NOMENCLATURE

A	area of bead
A_f	area of bead flute
A_w	area of bead web
B	width of panel
b	width of bead, width of tube, at panel middle plane
b_d	projection of diagonal width on panel mid plane (see Fig. 12-2)
b_f	width of bead flute
b_w	width of bead web
C.F.	correlation factor
d	diagonal width (see Fig. 12-2)
D_1, D_2, D_3	orthotropic plate stiffness coefficients in panel stability equations
D_1', D_2', D_3'	orthotropic plate stiffness coefficients in diagonal buckling equations
E	modulus of elasticity
E_{sec}	secant modulus
E_{tan}	tangent modulus
f	width of flat
f_b, f_c, f_s	bending, compression, shear stresses
f_i	stress intensity, octrahedral shear theory
f_{sflat}	maximum shear stress in flat (single sheet configurations only)
F_b, F_c, F_s	bending, compression, shear stresses at failure (prime denotes equivalent elastic stress)
F_{cb}, F_{cc}, F_{cs}	bending, compression, shear local buckling critical stresses of circular arc elements
F_i	stress intensity at failure (prime denotes equivalent elastic stress)
F_{sflat}	maximum shear stress in flat at failure
F_{cr}	critical stress (prime denotes equivalent elastic stress)

NOMENCLATURE (Cont'd)

F_{ccr}, F_{scr}	compression, shear critical stresses (prime denotes equivalent elastic stress)
F_{cy}	compression yield stress
F_{fc}, F_{fs}	compression, shear local buckling critical stresses of flat elements
F_{pl}	proportional limit stress, threshold of inelastic stress region
G	shear modulus
g	function of structural element geometry
h	bead height
h_d	height of diagonal (see Fig. 12-2)
h_f	depth of bead flute
h_w	arc height of bead web
h_z	(see Fig. 12-2)
I	moment of inertia of one bead or tube about panel mid plane axis
I_d	moment of inertia of panel cross section associated with diagonal width, d, about diagonal axis (see Fig. 12-2)
I_f	moment of inertia of bead flute about its centroid axis parallel to panel mid plane
I_w	moment of inertia of bead web about its centroid axis parallel to panel mid plane
$\bar{J}$	average torsional constant per unit width
k, k_s	buckling coefficients
L	Length of panel
M_x	panel center bending moment per unit width (in-lb/in.)
N_x	panel axial compression load, lb/in.
N_{xcr}	critical axial compression load for panel instability
N_{xdcr}	critical axial compression load for diagonal buckling

N_{xy}	panel shear load, lb/in.
N_{xycr}	critical shear load for panel instability
N_{xydcr}	critical shear load for diagonal buckling
n	shape factor in Ramberg-Osgood stress-strain law
p	pressure, psi; width of panel between crests of alternate beads (see Fig. 12-1)
Q	statical moment of one bead about panel mid plane axis
R	radius
R_b, R_c, R_s	stress ratios of actual stress to critical stress for bending, compression, shear (prime denotes equivalent elastic stress ratio)
R_f	radius of bead flute
R_w	radius of bead web
s	developed length of panel cross section over the width p
s_c	arc length of circular arc element of panel cross section
s_d	developed length of panel cross section associated with diagonal width, d
t	thickness
$\bar{t}$	equivalent extensional thickness
U	utilization factor (prime denotes equivalent elastic value)
$\bar{y}$	distance from panel mid plane to centroid of bead (circular arc) cross section
$\bar{y}_f, \bar{y}_w$	distance from panel mid plane to centroid of bead flute, web
y_o	panel center deflection produced by pressure load only
Z	panel curvature parameter in local shear buckling analysis

NOMENCLATURE (Cont'd)

α	half angle of circular bead arc
α_f	half angle of bead flute arc
α_w	half angle of bead web arc
β	effective aspect ratio of rectangular, orthotropic plate
$\gamma, \gamma_b, \gamma_c$	correlation factors used in bead crippling analysis
η, η_i	plasticity correction factor (numerical subscript, i, identifies equation used; see Eqs. 12-54)
η_c, η_s	plasticity correction factor for compression, shear
η_{sec}, η_{tan}	plasticity correction factors calculated from secant modulus, tangent modulus
θ	angle defining diagonal width, d (see Fig. 12-2)
θ_o	inclination of bead web radius from vertical at crest of bead (see Fig. 12-2)
θ_w	inclination of bead web chord from vertical (see Fig. 12-2)
ν, ν_x, ν_y	Poisson's ratio, subscripts x and y refer to principal directions in an orthotropic plate
σ_x, σ_y	normal stress in x and y directions
τ_{xy}	shear stress on an x or y face
ϕ	angle of bead web intersection with panel mid plane
ω	half angle of bead web arc intercepted by diagonal axis, d (see Fig. 12-2)

SUMMARY

A study was conducted to exploit the efficiency of curved elements in the design of lightweight structural panels under combined loads of axial compression, inplane shear, and bending. Governing analytical static strength and stability equations and material and geometric constraint equations were incorporated in a random search-type optimization computer program to identify minimum weight designs for several potentially efficient concepts. Buckling tests were conducted on subscale panels to identify local failure modes and provide for modification of local buckling theory where required. Full scale 40 x 40 inch (1 x 1 meter) panels were tested under combined loading to obtain failure data for correlation with theory. Modifications to failure theory were made as required. A nondestructive force-stiffness test technique was used in conjunction with the Moire' grid monitoring technique to provide extensive test data from a comparatively few test panels.

A summary of the total program (analysis, fabrication and test) is presented in document NASA CR-2514. The report presented herein is a supplement to the summary document and contains detailed analytical procedures for optimum panel design, static strength analyses, results of panel design studies, and correlation of theory with test results. Detailed descriptions of the fabrication development and of the panel tests are contained in supplementary documents NASA CR-132482, and NASA CR-132515, respectively.

The work reported herein has resulted in a verified analysis and design procedure for one of the panel configurations studied. Typical design curves for this configuration are presented. Comparison of test results with theory for the other three configurations shows poor agreement, and a verified design procedure for these concepts was not attained. The need for further analytical effort is discussed.

INTRODUCTION

For several years Langley Research Center and other NASA agencies have been investigating structural concepts which use elements with curved cross sections to develop beaded or corrugated skin panel structure as indicated in References 1 through 6. The curved sections exhibit high local buckling strength which leads to highly efficient structural concepts. These concepts can be applied where a lightly beaded external surface is aerodynamically acceptable or where the primary structure is protected by heat shields. The corrugated nature of the panels makes them especially attractive for high temperature application because controlled thermal growth is permitted which minimizes thermal stress. The technology resulting from this program is applicable to various formable materials and to many areas such as launch vehicles, space vehicles and hypersonic aircraft.

A study was conducted to develop lightweight structural panels designed for combined loads of axial compression, inplane shear, and bending due to lateral pressure. Governing analytical static strength and stability equations for panels under combined load, and material and geometric constraint equations were incorporated in a random search type optimization computer program described in Reference 7 to identify minimum weight designs for several potentially efficient concepts. However, in order for these concepts to realize their analytical potential, all of the significant failure modes had to be properly recognized and accounted for. Consequently, a major fabrication and test development effort was initiated. Buckling tests were conducted on subscale panels to identify local failure modes and provide data for the modification of local buckling theory where required. Full scale 40 x 40 inch (1 x 1 meter) panels were tested under combined loading to obtain large panel failure data for correlation with theory. A nondestructive force-stiffness test technique described in Reference 8, was used in conjunction with the Moire' grid monitoring technique to provide extensive test data from a comparatively few test panels. A summary of this study (analysis, fabrication and testing) is presented in document NASA CR-2514. Detailed descriptions of the fabrication development and of the panel tests are contained in supplementary documents NASA CR-132482 and NASA CR-132515 respectively.

The report presented herein describes the analytical methods developed for optimum design and for static strength analysis of beaded and tubular panels. Preliminary design trade studies were conducted to determine relative efficiencies of different panel configurations. From these studies four final panel designs were selected for further development. Correlation of the analysis with test data from local buckling specimens and from full scale panel tests of these four panel designs is presented and discussed.

11.0 DESIGN AND ANALYSIS PROCEDURES

The design/analysis procedure consists of the following basic tasks:

1) Identification of buckling and failure modes of beaded and tubular panels.

2) Development of analytical methods for predicting buckling and failure loads for the modes identified.

3) Incorporation of analytical equations into computer codes for optimum design (OPTRAN) and for panel strength prediction (PANAP).

4) After design, fabrication and testing of panel specimens, comparing the analysis with test results to determine if modifications are necessary to obtain the desired degree of correlation.

The results of the first two tasks constitute the static strength analysis, which is presented in detail in Section 12 of this document. The computer codes developed in the third task are discussed briefly in Sections 11.1 and 11.2. The results of the fourth task are discussed separately in Section 14, CORRELATION WITH TEST DATA.

11.1 Optimum Design (OPTRAN)

Minimum weight panel designs are obtained using a computer code called OPTRAN (OPTimization by RANdom search technique). This code was derived from experience with the Boeing developed AESOP program (Reference 11-1) in optimizing panel and cylinder designs. The random point search method of the AESOP program was further developed by Laakso (Reference 11-2) into the OPTRAN code. Designs are established by random selection of values for the dimensional parameters (thickness, bead spacing, radius, etc.) within specified search ranges. Observance of minimum gage or bead spacing design constraints is accomplished by proper specification of the search ranges. If a design is found that has lower weight than the best preceding design, failure mechanism constraints are then checked. If all constraints are satisfied then the design becomes

the current best design. The process is repeated until a specified number of good designs are found, which completes a search cycle. Design refinement is achieved by resizing the parameter search ranges and conducting another search cycle; the search cycles are repeated until the weight change between successive cycles is within a specified tolerance which signifies convergence to an acceptable optimum design. This search technique was found to be simple, reliable and adequate.

An individual OPTRAN code is specialized for each panel type by adding code modules describing panel geometry, section properties and failure mechanisms. OPTRAN may evaluate thousands of panel configurations in the process of arriving at a single optimum design. Therefore, for the sake of economy, static strength equations are coded in the simplest forms available consistent with accuracy. The static strength equations which are incorporated in the OPTRAN panel codes are discussed in detail in Section 12.

11.2 Strength Predictions (PANAP)

The PANAP (PANel Analysis Program) computer codes were developed under this program to obtain analytical strength predictions for each of the three basic panel types selected for final development in this program. These codes use the same static strength equations incorporated in OPTRAN. They give ultimate loads and panel stresses associated with each failure mode for a specific dimensional configuration and for any number of arbitrary load conditions. Input to the PANAP codes consists of geometric parameters describing the cross section and panel dimensions, and descriptions of load conditions. Geometric parameters may be obtained directly from an OPTRAN design, or may be measurements from test specimens. Load conditions are specified by the ratios of compression, shear, and lateral pressure. The option is available to specify the lateral pressure as a constant value. The PANAP codes are used to obtain the analytical panel strengths appearing in the final data correlations (Section 14.2).

12.0 STATIC STRENGTH ANALYSIS

The basis for panel design optimization is the static strength analysis. This analysis can be considered in five parts as follows:

1) Calculation of section properties and other geometric parameters needed for stress and stability analyses.

2) Stress analysis for determining detailed stress distributions as functions of applied loads and panel geometry.

3) Failure mode analysis to determine critical loads for panel general instability, local buckling, and material strength.

4) Interaction analysis for failure criteria under combined loads.

5) Plasticity corrections for modifying failure criteria when elastic failure mode analyses indicate failure stresses that are beyond the material proportional limit.

These parts of the static strength analysis are discussed in detail in the following subsections.

12.1 Section Properties

Panel Cross Section Geometry

Before calculations of panel stiffnesses can be made, a complete geometric description of the panel cross section is required. This description begins with the identification of the design parameters, the values of which are selected randomly as independent variables in the OPTRAN code to establish a panel design. From these independent design parameters a more extensive set of dependent geometric parameters are calculated prior to calculation of stiffnesses and other section properties.

Independent Parameters - The independently selected design parameters listed below are identified in Figure 12-1 for the various panel configurations.

Type 1 and Type 2:

t, R, α, f

Type 1A and Type 2A:

$t, b, h, b_f, h_f, f, \phi$

Dependent Parameters - The necessary additional geometric parameters are calculated from the independent design parameters according to the following equations. These are identified in Figure 12-1 and Figure 12-2.

Type 1 and Type 2:

$$\begin{aligned} b &= 2R \sin \alpha \\ p &= b + f \\ h &= R(1 - \cos \alpha) \\ s &= 2R\,\alpha + f \end{aligned} \tag{12-1}$$

$$\bar{y} = R \left(\frac{\sin \alpha}{\alpha} - \cos \alpha \right)$$

Type 1 only:

$$b_d = p - 2R \sin \theta \quad \left(0 \leq \theta \leq \frac{2}{3} \alpha\right)$$

$$h_d = 2R(\cos \theta - \cos \alpha)$$

$$\begin{aligned} d &= (b_d^2 + h_d^2)^{1/2} \\ h_z &= f\, h_d/d \\ \omega &= \cos^{-1} (b_d/d) - \theta \\ s_d &= 2R(\alpha - \theta) + f \end{aligned} \tag{12-2}$$

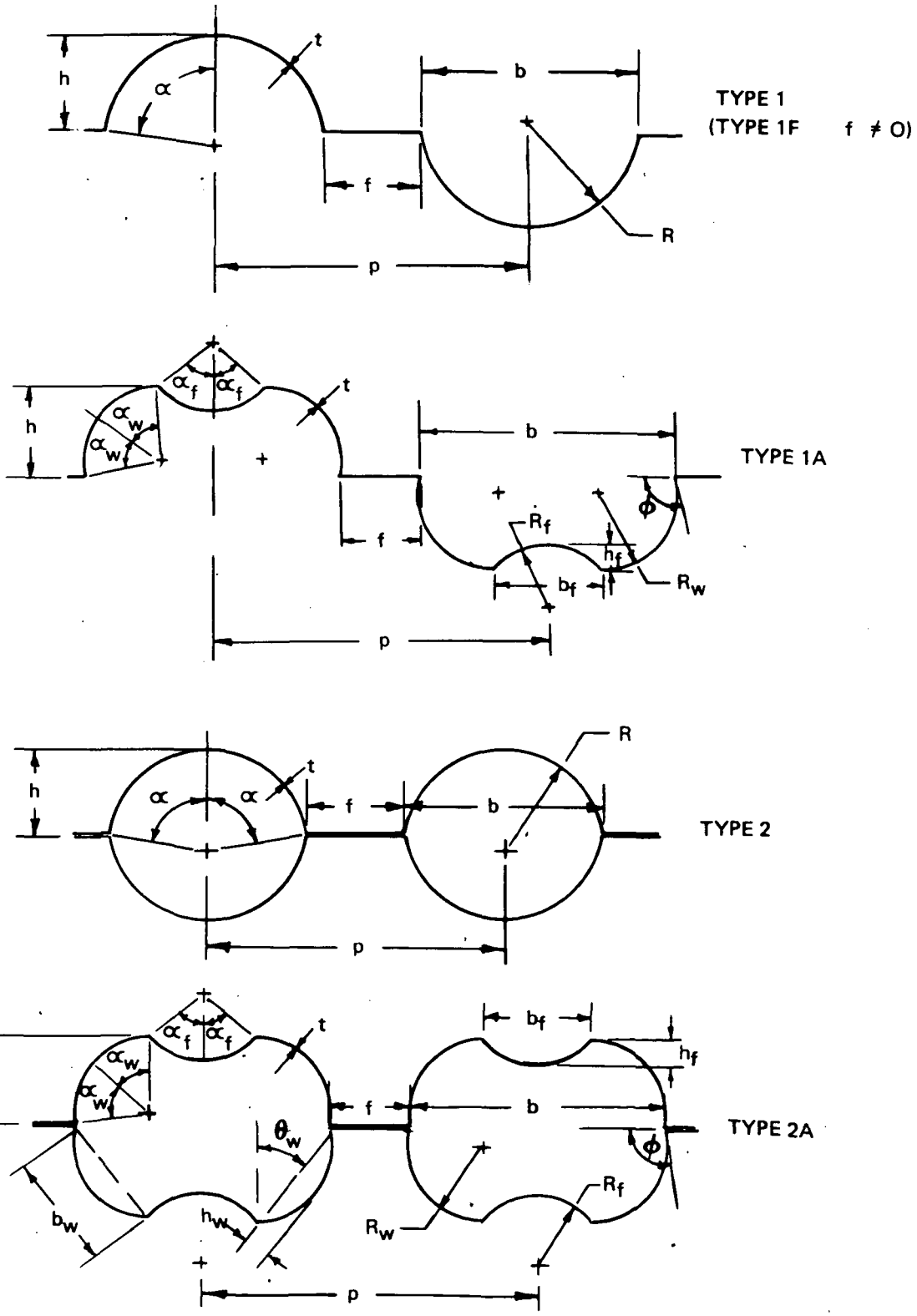

Figure 12-1: BASIC GEOMETRY OF BEADED AND TUBULAR PANEL CONFIGURATIONS

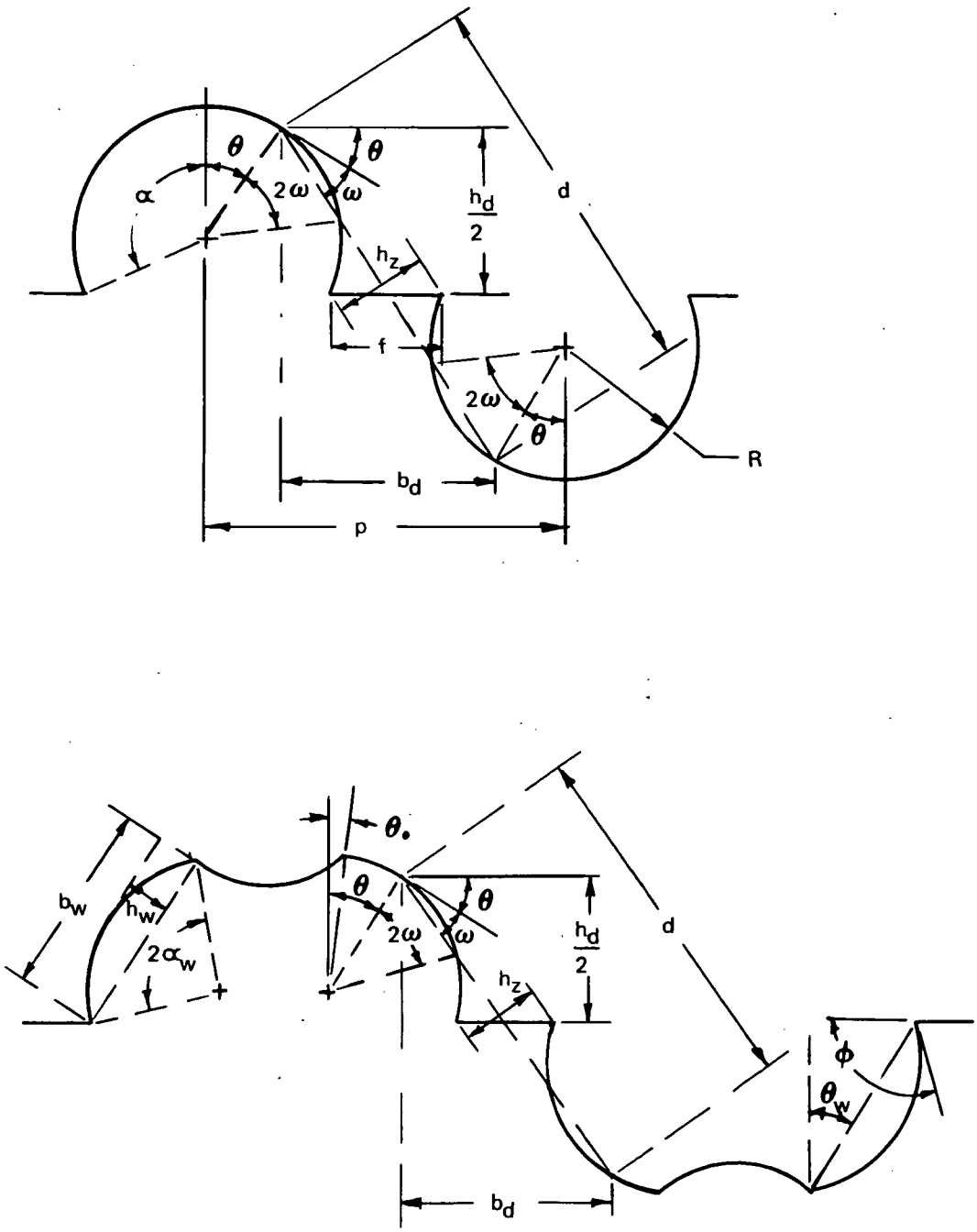

Figure 12-2: DETAILED GEOMETRIES OF SINGLE-SHEET CONFIGURATIONS FOR CALCULATION OF SECTION PROPERTIES

Type 1A and 2A:

$$
\begin{aligned}
p &= b + f \\
b_w &= \left[h^2 + \frac{1}{4}(b - b_f)^2\right]^{1/2} \\
\theta_w &= \cos^{-1}(h/b_w) \\
\alpha_w &= \phi - \pi/2 + \theta_w \\
\alpha_f &= 2\tan^{-1}(2h_f/b_f) \\
h_w &= \tfrac{1}{2} b_w \tan(\alpha_w/2) \\
R_w &= h_w/(1 - \cos\alpha_w) \\
R_f &= h_f/(1 - \cos\alpha_f) \\
\bar{y}_w &= h/2 + R_w\left(\frac{\sin\alpha_w}{\alpha_w} - \cos\alpha_w\right)\cdot\frac{(b - b_f)}{2b_w} \\
\bar{y}_f &= h - R_f\left(\frac{\sin\alpha_f}{\alpha_f} - \cos\alpha_f\right)
\end{aligned}
\qquad (12\text{-}3)
$$

Type 1A only:

$$
\begin{aligned}
\theta_o &= \phi - 2\alpha_w \quad (\theta_o \geq 0) \\
b_d &= p - 2R_f \sin\alpha_f + 2R_w(\sin\theta_o - \sin\theta), \quad (\theta_o \leq \theta \leq \alpha_w) \\
h_d &= 2R_w(\cos\theta - \cos\phi) \\
d &= (b_d^2 + h_d^2)^{1/2} \\
h_z &= f\, h_d/d \\
\omega &= \cos^{-1}(b_d/d) - \theta \\
s_d &= 2R_w(\phi - \theta) + f
\end{aligned}
\qquad (12\text{-}4)
$$

Bead and Tube Properties

Areas, statical moments, and moments of inertia of individual beads and tubes are required for determining panel stiffnesses and for other purposes in the analysis. These are calculated as follows.

Type 1:

$$A = 2\alpha Rt$$

$$Q = A\bar{y}$$

$$I = R^3 t \left(\alpha + \sin\alpha \cos\alpha - \frac{2\sin^2\alpha}{\alpha}\right) + A\bar{y}^2 \qquad (12\text{-}5)$$

Type 2:

$$A = 2\alpha Rt$$

$$I = 2\left[R^3 t\left(\alpha + \sin\alpha \cos\alpha - \frac{2\sin^2\alpha}{\alpha}\right) + A\bar{y}^2\right] \qquad (12\text{-}6)$$

Type 1A:

$$A_w = 4 R_w \alpha_w t$$

$$A_f = 2R_f \alpha_f t$$

$$Q = A_w \bar{y}_w + A_f \bar{y}_f$$

$$I_f = R_f^3 t \left(\alpha_f + \sin\alpha_f \cos\alpha_f - \frac{2\sin^2\alpha_f}{\alpha_f}\right) \qquad (12\text{-}7)$$

$$I_{w1} = R_w^3 t \left(\alpha_w + \sin\alpha_w \cos\alpha_w - \frac{2\sin^2\alpha_w}{\alpha_w}\right) \qquad (12\text{-}7)$$

$$I_{w2} = R_w^3 t \left(\alpha_w - \sin\alpha_w \cos\alpha_w\right)$$

$$I_w = (I_{w1} + I_{w2}) + (I_{w1} - I_{w2}) \cos(\pi - 2\theta_w)$$

$$I = I_f + I_w + A_f \bar{y}_f^2 + A_w \bar{y}_w^2$$

Type 2A:

$$A_w = 4R_w \alpha_w t$$

$$A_f = 2R_f \alpha_f t$$

$$I_f = R_f^3 t \left(\alpha_f + \sin\alpha_f \cos\alpha_f - \frac{2\sin^2\alpha_f}{\alpha_f}\right)$$

$$I_{w1} = R_w^3 t \left(\alpha_w + \sin\alpha_w \cos\alpha_w - \frac{2\sin^2\alpha_w}{\alpha_w}\right) \qquad (12\text{-}8)$$

$$I_{w2} = R_w^3 t\,(\alpha_w - \sin\alpha_w \cos\alpha_w)$$

$$I_w = (I_{w1} + I_{w2}) + (I_{w1} - I_{w2}) \cos(\pi - 2\theta_w)$$

$$I = 2(I_f + I_w + A_f \bar{y}_f^2 + A_w \bar{y}_w^2)$$

Orthotropic Plate Bending Stiffness Coefficients

For an orthotropic plate the bending stiffness coefficients are given by Timoshenko in Reference 12-1, pp. 403-404, as follows:

$$D_1 = (EI)_x/(1 - \nu_x\nu_y)$$

$$D_2 = (EI)_y/(1 - \nu_x\nu_y)$$

$$D_3 = \frac{1}{2}(\nu_x D_2 + \nu_y D_1) + 2(GI)_{xy} \qquad (12\text{-}9)$$

For the isotropic case these simplify to,

$$D_1 = D_2 = D_3 = Et^3/12(1 - \nu^2)$$

and

$$\nu_x = \nu_y = \nu \qquad (12\text{-}10)$$

Substituting these values into the more general expression above for the twisting rigidity,

$$D_3 = \nu D + 2(GI)_{xy}$$

$$= \frac{\nu(EI)_x}{(1-\nu^2)} + \frac{(1-\nu)(EI)_{xy}}{(1-\nu^2)} = \frac{Et^3}{12(1-\nu^2)} \qquad (12\text{-}11)$$

which is satisfied only if

$$(EI)_x = (EI)_{xy} = \frac{Et^3}{12} \tag{12-12}$$

From the foregoing discussion it may be concluded that I in the term $2(GI)_{xy}$ of D_3 is given by

$$I = \frac{t^3}{12} \tag{12-13}$$

If the torsional rigidity of the flat, isotropic plate is represented by the torsional constant per unit width from Roark, (Reference 12-2, p. 176)

$$\bar{J} = \frac{K}{U} = \frac{t^3}{3}$$

then

$$I = \bar{J}/4 \tag{12-14}$$

For the single sheet panel configurations, types 1 and 1A, the torsional constant per unit width is derived from the foregoing equations:

$$\bar{J} = \frac{t^3}{3} \cdot \frac{s}{p} \tag{12-15}$$

where p is the width between crests of alternate beads, i.e., one-half the full pitch, and s is the developed length of the beaded cross section over the width p.

For the two-sheet, tubular configurations, types 2 and 2A, the effective torsional constant must be derived by considering the case of springs in series where the overall stiffness is the inverse of the sum of the flexibilities, rather than the sum of the stiffnesses. Therefore, although the torsional rigidity of the tubes is high, the overall twisting stiffness of the panels is low because of the low torsional rigidity of the flats. Considering the tubes to be rigid in comparison to the flats, the average torsional constant per unit width is given by:

$$\bar{J} = \frac{(2t)^3}{3} \cdot \frac{b + f}{f} \qquad (12\text{-}16)$$

where b is the width of the tube and f is the width of the flat.

According to Timoshenko (Reference 12-1, p. 404) tests show that ν_x and ν_y in Equations (12-9) can usually be taken as zero. This is assumed to be the case for both the beaded and the tubular panel configurations. Therefore, the orthotropic plate bending stiffness coefficients reduce to

$$D_1 = (EI)_x$$

$$D_2 = (EI)_y$$

$$D_3 = 2(GI)_{xy} = \frac{E\bar{J}}{4(1+\nu)} \qquad (12\text{-}17)$$

Plate bending stiffness coefficients for the beaded and tubular panels are determined from Equations (12-17) by calculating effective bending stiffnesses per unit width for $(EI_x$ and $(EI)_y$ from the panel geometries, and obtaining $\bar{J}$ from Equation (12-15) and Equation (12-16). Considering the x axis to be the direction of the principal stiffness (i.e., parallel to the longitudinal axes of the beads and tubes) these are:

Type 1 and Type 1A

$$D_1 = \frac{EI}{p}$$

$$D_2 = \frac{Et^3}{12(1-\nu^2)} \cdot \frac{p}{s}$$

$$D_3 = \frac{Et^3}{12(1+\nu)} \cdot \frac{s}{p} \qquad (12\text{-}18)$$

Type 2 and Type 2A:

$$D_1 = \frac{EI}{p}$$

$$D_2 = \frac{D_1^* D_2^* (b+f)}{D_1^* f + D_2^* b}$$

$$D_3 = \frac{2Et^3}{3(1+\nu)} \cdot \frac{(b+f)}{f} \qquad (12\text{-}19a)$$

where $$D_2^* = \frac{2Et^3}{3(1-\nu^2)} \qquad (12\text{-}19b)$$

and, for Type 2,

$$D_1^* = \frac{2\sin\alpha}{c} \cdot \frac{Et^3}{12(1-\nu^2)}$$

$$c = \alpha - \frac{(\sin\alpha - \alpha\cos\alpha)^2}{\left[\alpha(\tfrac{1}{2} + \cos^2\alpha) - \frac{3}{2}\sin\alpha\cos\alpha\right]} \qquad (12\text{-}19c)$$

and, for Type 2A;

$$D_1^* = \frac{b}{\left[C_{11} - \frac{(C_{12})^2}{C_{22}}\right]} \cdot \frac{Et^3}{12(1-\nu^2)}$$

$$C_{11} = 2\alpha_w R_w + \alpha_f R_f \qquad (12\text{-}19d)$$

$$C_{12} = R_w^2 \sin\phi(1-\cos 2\alpha_w) + hR_f\alpha_f - R_f^2 \sin\alpha_f(1-\cos\alpha_f)$$

$$C_{22} = R_w^2 \sin^2\phi(\alpha_w - \tfrac{1}{4}\sin 4\alpha_w) + h^2 R_f \alpha_f - 2hR_f^2 \sin\alpha_f(1-\cos\alpha_f) + R_f^3 \sin^2\alpha_f\left(\frac{\alpha_f}{2} - \tfrac{1}{4}\sin 2\alpha_f\right)$$

The stiffness coefficients for the single sheet, beaded configurations, Equations (12-18) agree with the approximate formulas given by Lekhnitskii in Reference 12-3, p. 294, for corrugated plates. In Equations (12-19c) the expression for c is an approximation which is accurate for R/t ratios and bead angles in the ranges of interest (i.e., $R/t \geq 20$ and $\alpha \geq 30^\circ$). The expression for D_3 in Equation (12-19a) is derived on the assumption

that the tubes are rigid in torsion relative to the flats, and is valid only if the tube cross section remains undistorted. Distortion of the tube cross section can greatly increase the apparent torsional flexibility of the tubes, thus causing the effective value of D_3 to be much lower than the value given by this equation. Such distortion of the tube cross section was observed in tests of the type 2A panels. (See Section 14.2 and Volume 3, Testing.)

Orthotropic plate bending stiffness coefficients for that part of the panel associated with the diagonal width, d, of the single sheet configuration (see Figure 12-2) are needed to analyze the diagonal mode of buckling. These are calculated as follows.

Type 1 and Type 1A:

$$D_1' = \frac{EI_d}{d}$$

$$D_2' = \frac{Et^3}{12(1-\nu^2)} \cdot \frac{d}{s_d} \qquad (12\text{-}20a)$$

$$D_3' = \frac{Et^3}{12(1+\nu)} \cdot \frac{s_d}{d}$$

where, $$I_d = 2I_c + I_z + \frac{dt^3}{12(1-\nu^2)}$$

and, for Type 1:

$$I_c = R^3 t\ (\omega - 3\sin\omega\cos\omega + 2\omega\cos^2\omega)$$

$$I_z = t\left[f + 2R(\alpha - 2\omega - \theta)\right] \cdot \frac{h_z^2}{12} \qquad (12\text{-}20b)$$

and, for Type 1A:

$$I_c = R_w^3 t(\omega - 3\sin\omega\cos\omega + 2\omega\cos^2\omega)$$

$$I_z = t\left[f + 2R_w(\phi - 2\omega - \theta)\right] \cdot \frac{h_z^2}{12} \qquad (12\text{-}20c)$$

12.2 Stress Analysis

Stresses are calculated at the panel center from the cross section geometry, the panel edge loadings and the panel bending moments, using elementary theory as follows.

Axial Compression

Calculated at panel centroidal axis

$$f_c = N_x/\bar{t} \tag{12-21}$$

where, for panel Type 1 and Type 1A,

$$\bar{t} = ts/p$$

and, for panel Type 2 and Type 2A,

$$\bar{t} = 2ts/p$$

Bending

For highly orthotropic panels deflections and bending moments are analyzed with sufficient accuracy using beam column theory rather than the more complicated orthotropic plate analysis. Timoshenko (Reference 12-1, pp. 29-30) derives an amplification factor for approximate analysis of beam column deflections which is used here. With a uniform lateral load the approximate analysis is accurate within one-half of one percent for values of the axial load less than the column critical load. The panel center bending moment is given by,

$$M_x = pL^2/8 + N_x y_o/(1 - N_x/N_{xcr}) \tag{12-22}$$

The first term in the expression is the center bending moment for a beam with simple end supports and a uniform pressure load, p. The second term is the column bending moment produced by the axial load acting on the total panel center deflection where y_o is the center deflection produced by the pressure load p alone plus an assumed initial eccentricity, i.e.,

$$y_o = 5pL^4/384\ D_1 + .001L \qquad (12\text{-}23)$$

The denominator of the second term in Equation (12-22) is the amplification factor which simulates the beam-column effect. As the axial compression load, N_x, approaches the column critical load, N_{xcr}, the denominator approaches zero and the second term in the expression for bending moment increases without limit. The shear load, N_{xy}, is not considered in calculating the amplification factor. The characteristic mode shape for general instability in shear of these panels has several half waves across the panel width. Therefore, very little coupling exists between this mode shape and the deflected shape due to the lateral pressure, which consists essentially of a single half wave. Because of this small degree of coupling, and the generally smaller magnitude of shear load compared to compression in panel design loads, the amplification effect of the shear load has been assumed negligible.

The compression stress due to bending is calculated at the extreme fiber of the bead or tube.

$$f_b = M_x\ cE/D_1 \qquad (12\text{-}24)$$

where, for panel Type 1 and Type 1A,

$$c = h$$

and for panel Type 2 and Type 2A,

$$c = h + t/2.$$

Shear

Shear stress is assumed uniformly distributed throughout the sheet, or sheets, which form the panel.

Type 1 and Type 1A:

$$f_s = N_{xy}/t \qquad (12\text{-}25)$$

Type 2 and Type 2A:

$$f_s = N_{xy}/2t$$

The maximum shear stress in the flats, due to bending (single sheet configurations only), is at the panel ends. This is calculated conservatively from an approximate formula derived from the assumption of sinusoidal distribution of panel longitudinal bending moment.

Type 1 and Type 1A only:

$$f_{s_{flat}} = f_s + \pi M_x EQ/2D_1Lt \qquad (12\text{-}27)$$

where M_x is the maximum bending moment at the panel center and L is the panel length.

Stress Intensity

Stress intensity is determined from octohedral shear theory as given by Nadai (Reference 12-4). It is calculated at the extreme fiber of the bead or tube at the panel center.

$$f_{i_{max}} = \left[(f_c + f_b)^2 + 3f_s^2\right]^{1/2} \qquad (12\text{-}28)$$

12.3 Failure Mode Analysis

Panel General Instability

Compression - The critical axial compression load for panel instability is determined from the wide-column Euler buckling equation:

$$N_{xcr} = \pi^2 \eta_5 D_1/L^2 \qquad (12\text{-}29)$$

This equation is sufficiently accurate for highly orthotropic panels where both the transverse bending and twisting stiffness coefficients, D_2 and D_3,

are very small in comparison to the longitudinal bending stiffness coefficient, D_1. All of the panel configurations being considered here satisfy this criterion. The plasticity coefficient, η_5 in Equation (12-29) is a reduction factor applied when critical stresses are greater than the proportional limit stress. For the linear elastic case it is equal to unity. A detailed discussion of plasticity corrections is given in Section 12.5.

The wide column Euler buckling load also appears in the amplification factor for calculating panel bending moment, Equation (2-22). In this case a different plasticity correction factor is used because η_5 is a function of the bending stress, which is not yet available. Therefore,

$$N_{xcr} = \pi^2 \eta_1 D_1 / L^2 \qquad (12\text{-}29a)$$

Shear - The critical shear load for panel general instability is taken from Timoshenko (Reference 12-1, p. 407):

$$N_{xycr} = \eta_2 (4k/L^2)(D_1^3 D_2)^{1/4} \qquad (12\text{-}30)$$

where k is a function of

$$\beta = (L/B)\ (D_2/D_1)^{1/4}$$

$$1/\Theta = D_3/(D_1 D_2)^{1/2}$$

and is taken from the curves in the reference. Equation (12-30) is valid for $\Theta \geq 1$ and for $\beta \leq 1$, which are satisfied for all panel configurations being considered here.

Local Instability

Local instability is defined here as buckling of one or more elements of the panel cross section with buckle half-wave lengths which are small compared to the panel length. Specifically, the modes considered are: buckling of flat elements occurring between adjacent beads or tubes; buckling of circular arc elements of the bead or tube cross section, referred to as

bead crippling; and buckling of portions of the panel cross section consisting of adjacent circular arcs with intermediate flat where applicable, referred to as diagonal buckling.

Flat Buckling - Flat elements are analyzed for local instability as long, simply supported, isotropic plates using equations given by Timoshenko and Gere (Reference 12-1). The critical compression stresses for the single sheet, beaded configurations are:

Type 1 and Type 1A;

$$F_{fc} = \pi^2 \eta_4 E t^2 / [3f^2(1-\nu^2)]$$

$$F_{fs} = 5.35\pi^2 \eta_4 E t^2 / [12f^2(1-\nu^2)] \qquad (12\text{-}31)$$

The critical compression stresses for the two-sheet, tubular configurations are:

Type 2 and Type 2A:

$$F_{fc} = 4\pi^2 \eta_4 E t^2 / [3f^2(1-\nu^2)]$$

$$F_{fs} = 5.35\pi^2 \eta_4 E t^2 / [3f^2(1-\nu^2)] \qquad (12\text{-}32)$$

Bead Crippling - Circular arc elements of the panel cross section are analyzed for local instability in compression and bending using equations derived from a classical solution with correlation factors presented by NASA in Reference 12-5.

$$F_{cc} = 0.82\eta_3 E(t/R)^{1.19}$$

$$F_{cb} = 0.77\eta_3 E(t/R)^{1.15} \qquad (12\text{-}33)$$

These equations are approximations to the analyses given in Reference 12-5 which are valid for the R/t range of interest in these panels (i.e., $20 \leq R/t \leq 120$). Plots comparing Equations (12-33) with the NASA analyses over this range are shown in Figure 12-3.

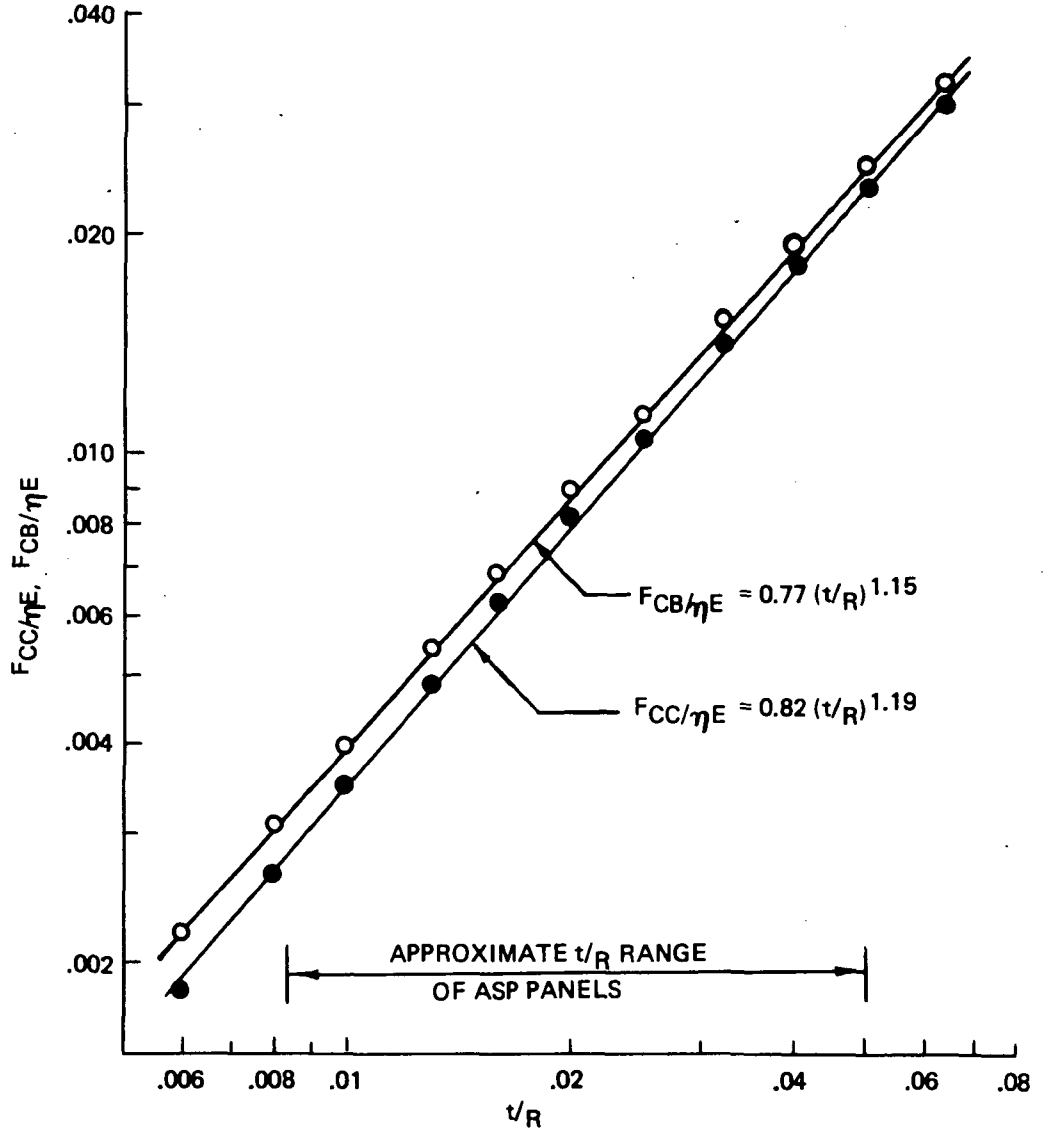

Figure 12-3: BUCKLING OF CYLINDRICAL SHEETS SUBJECT TO AXIAL COMPRESSION AND BENDING

The critical stress for local instability in shear is taken from Gerard and Becker (Reference 12-6):

$$F_{cs} = \eta_2 G k_s (t/s_c)^2 \qquad (12\text{-}34)$$

where,

$$k_s = 4Z^{.514}$$

$$Z = (s_c^2/Rt)\ (1-\nu^2)^{1/2}$$

The expression given here for k_s is an approximation to the curve given in Reference 12-6 for an infinitely long, simply supported, cylindrical plate. The approximation is accurate for values of $Z \geq 50$, which is satisfied for all panel configurations considered here.

For the fluted panel configurations, Type 1A and Type 2A, critical bead crippling stresses are calculated separately for the web and flute portions of the bead, using Equations (12-35) and (12-36). The web portion refers to the convex sidewalls of the bead, and the flute is the concave portion at the crest of the bead.

Diagonal Buckling - The diagonal buckling mode is analyzed as a long, simply supported, orthotropic plate, using equations from Timoshenko and Gere (Reference 12-1). The width of the plate, d, is made variable within specified limits of the angle Θ, as indicated in Figure 12-2 and in Equations (12-2) and (12-4), until the minimum value of the critical compression load is found using Equation (12-35a). The value of d is then fixed, and the critical load in shear is determined from Equation (12-35b).

$$N_{xdcr} = \eta_3 (2\pi^2/d^2)\ (\ D_1'D_2' + D_3')\ (ds/bs_d) \qquad (12\text{-}35a)$$

$$N_{xydcr} = \eta_2 (4k/d^2)[D_1'(D_2')^3]^{1/4} \qquad (12\text{-}35b)$$

where k is a function of

$$\beta = (d/L)(D_1'/D_2')^{1/4}$$

$$1/\Theta = D_3'/(D_1'D_2')^{1/2}$$

and is taken from the curves given in Reference 12-1.

Material Strength

The criterion for material strength used in the analysis is that the maximum stress intensity in the panel must not exceed the compression yield strength of the material.

12.4 Compression - Shear Interaction

The standard interaction equation for buckling failure of panels under combined loads of axial compression and shear is:

$$R_c + R_s^2 = 1 \qquad (12\text{-}36)$$

where R_c and R_s are stress ratios of the actual compression and shear stresses in the panel at failure under the combined load to the critical stresses in pure axial compression and in pure shear, respectively. This equation is used for all buckling failure modes, with the stress ratios defined in each case as follows:

Panel General Instability -

$$R_c = N_x/N_{xcr}$$
$$R_s = N_{xy}/N_{xycr} \qquad (12\text{-}37)$$

Local Instability -

Flat Buckling:

$$R_c = f_c/F_{fc}$$
$$R_s = f_s/F_{fs} \qquad (12\text{-}38a)$$

Bead Crippling:

$$R_c \approx f_c/F_{cc} + f_b/F_{cb}$$

$$R_s \approx f_s/F_{cs} \qquad (12\text{-}38b)$$

Diagonal Buckling:

$$R_c \approx N_x/N_{xdcr}$$

$$R_s \approx N_{xy}/N_{xydcr} \qquad (12\text{-}38c)$$

12.5 Plasticity Corrections

Procedure

Critical buckling stresses of structural elements can usually be expressed by equations of the general form,

$$F_{cr} = k\eta Eg \qquad (12\text{-}39)$$

where k is a constant, E is the elastic modulus of the material, and g is a function of the element geometry. The plasticity correction factor, η, is dependent on the material stress-strain characteristics and on the mechanism of buckling. When F_{cr} is less than the proportional limit stress, η is equal to unity and the equation reduces to the familiar elastic form. When F_{cr} is greater than the proportional limit stress the failure is inelastic. Since η is then a function of the stress, Equation (12-39) becomes transcendental. Iterative solutions of this equation tend to diverge unless special procedures are used, and even then, convergence is likely to be slow and unreliable. An alternate method of solution is to rewrite the equation in its equivalent elastic form,

$$F_{cr}/\eta = F_{cr}' = kEg \qquad (12\text{-}40)$$

F_{cr}' is an equivalent elastic failure stress which is greater than the actual failure stress, F_{cr}, whenever it is greater than the proportional limit stress, i.e.,

$$F_{cr}' > F_{cr} > F_{PL}$$

Since η is a specified function of stress, a plasticity correction curve of equivalent elastic stress, $F' = F/\eta$, versus actual stress, F, can be constructed.

Some typical plasticity correction curves of the type just described are shown schematically in Figure 12-4. The curves identified by η_{tan} and η_{sec} are derived from tangent and secant moduli of the material,

$$\eta_{tan} = E_{tan}/E, \quad \eta_{sec} = E_{sec}/E \tag{12-41}$$

These two curves represent maximum and minimum values of the plasticity correction factor. Other plasticity correction factors, represented by $\eta=\eta(\eta_{tan},\eta_{sec})$ in the figure, are functions of the tangent and secant moduli and the curves will always lie between these two extremes. [Entering this figure with the ordinate F'_{cr}, as would be calculated from Equation (12-40), the actual failure stress, F_{cr}, is determined by the abscissa (see dotted line).]

Critical loads or stresses for cases of compression alone, or of shear alone, are defined explicity by equations similar to Equation (12-39). In these cases it is a simple matter to use the appropriate plasticity correction curve as just described. However, failure under combined loading is usually defined by an interaction equation, such as Equation (12-36). The application of plasticity corrections in this type of failure analysis is complicated by the fact that different plasticity correction curves apply to determining critical stresses in compression alone and in shear alone. Furthermore, the equivalent elastic stress at which the curves of Figure 12-4 are entered is not the critical value in either compression alone or in shear alone, but is a function of both the compression and shear stresses at failure under the combined load.

Figure 12-5 illustrates the procedure used to apply plasticity corrections to the combined load failure analysis. The interaction equation is of the form

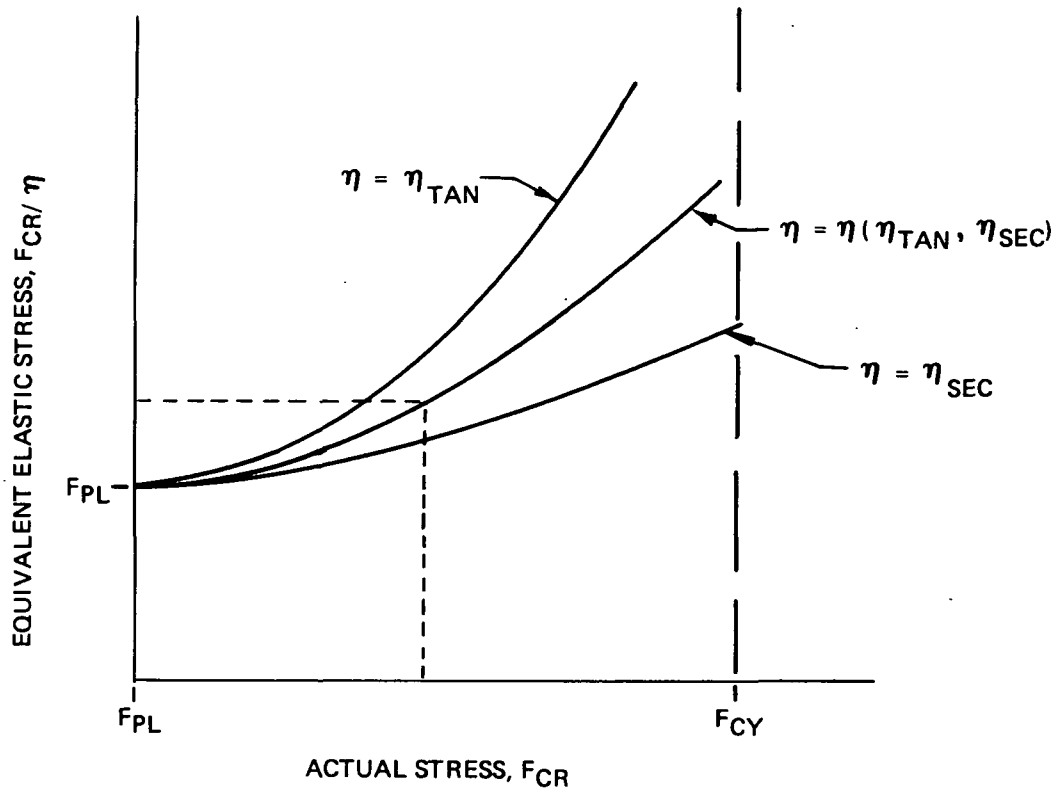

Figure 12-4: PLASTICITY CORRECTION CURVES

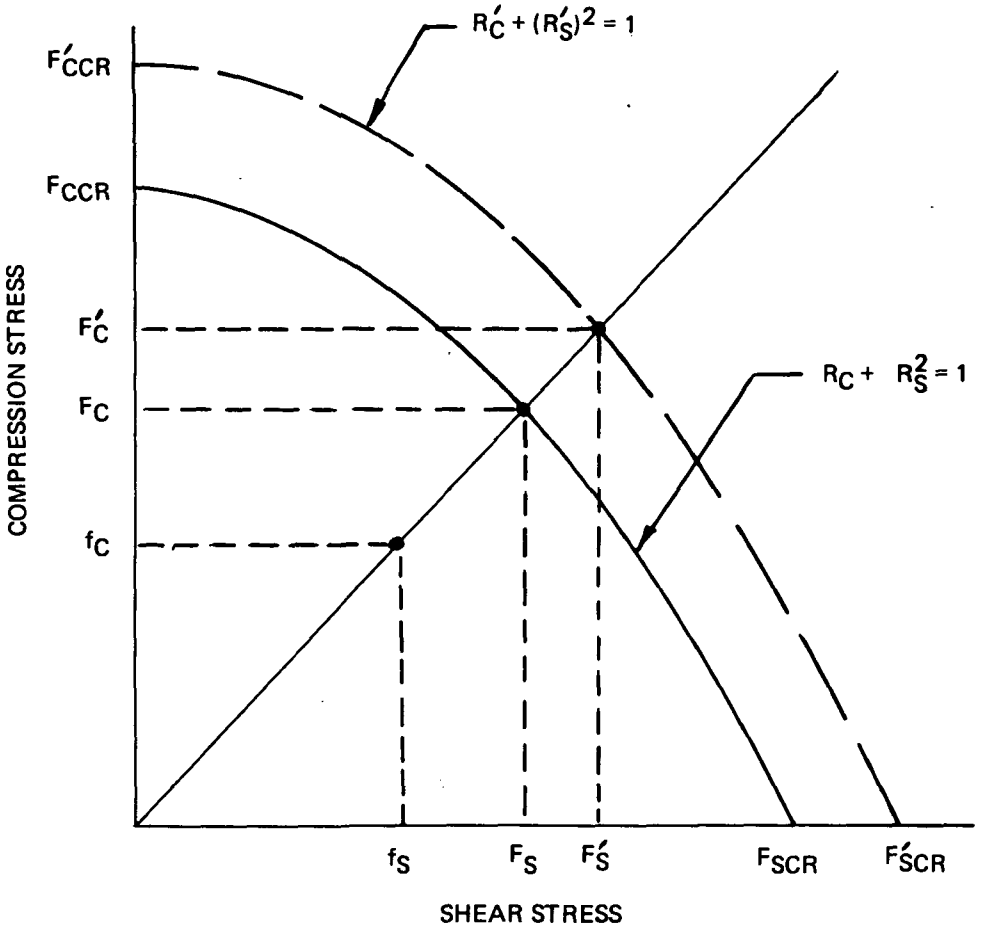

Figure 12-5: PLASTICITY CORRECTIONS TO COMBINED LOAD FAILURE ANALYSIS

$$R_c + R_s^2 = 1 \tag{12-42}$$

where R_c and R_s are stress ratios of actual stress to critical stress for pure compresssion and for pure shear, respectively. The point (f_c, f_s), in the figure, represents the actual compression and shear stresses existing under a specified load condition. The diagonal straight line passing through this point from the origin represents other stress levels produced by varying the load intensity while maintaining a constant ratio of compression stress to shear stress, i.e.,

$$f_c/f_s = \text{constant}. \tag{12-43}$$

Two curves are shown in the figure. The dashed curve, with end points F'_{ccr} and F'_{scr}, gives equivalent elastic failure stresses, F'_c and F'_s. The solid curve, with end points F_{ccr} and F_{scr}, gives the true, inelastic failure stresses, F_c and F_s. That is, F_c and F_s are the predicted actual failure stresses if the load intensity is increased such that f_c and f_s increase in conformity with Equation (12-43).

From Figure 12-5 and the preceding discussion the following relationships are established:

$$\begin{aligned} F'_{ccr} &= F_{ccr}/\eta_c \\ F'_{scr} &= F_{scr}/\eta_s \\ R'_c &= \eta_c R_c \\ R'_s &= \eta_s/R_s \\ F'_c &= F_c/\eta \\ F'_s &= F_s/\eta \end{aligned} \tag{12-44}$$

R'_c and R'_s are critical stress ratios based on the equivalent elastic critical stresses, F'_{ccr} and F'_{scr}. The plasticity correction factors η_c and η_s, for compression alone and for shear alone, are functions of the failure stresses, F_c and F_s. The stress intensity, as determined from octahedral shear theory (Reference 12-4), is used to represent the biaxial stress state

in calculating the plasticity correction factors. Finally, η is the unknown plasticity correction factor for the combined load failure.

The procedure for determining F_c, F_s, and η is outlined in the following steps:

1) Calculate equivalent elastic critical stresses, F'_{ccr} and F'_{scr}, from the elastic form of the buckling equations, Equation (12-40).

2) Calculate equivalent elastic stress ratios:

$$R'_c = f_c/F'_{ccr}$$
$$R'_s = f_s/F'_{scr} \qquad (12\text{-}45)$$

3) Calculate the equivalent elastic utilization factor for the combined load:

$$U' = 1/2[R'_c + \left\{(R'_c)^2 + 4(R'_s)^2\right\}^{1/2}] \qquad (12\text{-}46)$$

4) Calculate equivalent elastic failure stresses for the combined load:

$$F'_c = f_c/U'$$
$$F'_s = f_s/U' \qquad (12\text{-}47)$$

5) Calculate equivalent elastic stress intensity for the biaxial stress state represented by F'_c and F'_s:

$$F'_i = [(F'_c)^2 + 3(F'_s)^2]^{1/2} \qquad (12\text{-}48)$$

6) Enter the appropriate plasticity correction curve for compression buckling with F'_i as ordinate, determine F_i from abscissa, then calculate η_c:

$$\eta_c = F_i/F'_i \qquad (12\text{-}49)$$

7) Repeat step 6 using the appropriate plasticity correction curve for shear buckling to determine η_s.

8) Calculate true (inelastic) stress ratios:

$$R_c = R'_c/\eta_c$$
$$R_s = R'_s/\eta_s \qquad (12\text{-}50)$$

9) Calculate true (inelastic utilization factor:

$$U = 1/2\ [R_c + (R_c^2 + 4\ R_s^2)^{1/2}] \qquad (12\text{-}51)$$

10) Calculate true (inelastic) failure stresses for the combined load:

$$F_c = f_c/U$$

$$F_s = f_s/U \qquad (12\text{-}52)$$

11) If desired, calculate the plasticity correction factor for combined load failure:

$$\eta = U'/U \qquad (12\text{-}53)$$

Plasticity Correction Factors

The plasticity correction factors used in the various failure mode equations have been identified by numerical subscripts from 1 through 5. These are defined explicitly in the following equations as functions of the tangent and secant values:

$$\eta_1 = \eta_{tan} = E_{tan}/E \qquad \text{(Ref. 12-7)}$$

$$\eta_2 = \eta_{sec} = E_{sec}/E \qquad \text{(Ref. 12-6)}$$

$$\eta_3 = (\eta_{tan}\eta_{sec})^{1/2} \qquad \text{(Ref. 12-5)}$$

$$\eta_4 = \eta_{sec}\left[1/2 + 1/2\ [1/4 + (3\eta_{tan}/4\eta_{sec})]^{1/2}\right] \qquad \text{(Ref. 12-6)}$$

$$\eta_5 = \left[\frac{F_c^{\,2}\eta_{tan}^{\,2} + F_b^{\,2}\eta_{sec}^{\,2}}{F_c^{\,2} + F_b^{\,2}}\right]^{1/2} \qquad \text{(Ref. 12-8)} \qquad (12\text{-}54)$$

The tangent and secant moduli of the material are obtained from the following equations which are derived from a modified Ramberg-Osgood stress-strain law.

$$E_{tan} = \frac{F_i}{(F_i/E + n[.002(F_i/F_{cy})^n - .00001]}$$

$$E_{sec} = \frac{F_i}{(F_i/E + .002(F_i/F_{cy})^n - .00001)} \qquad (12\text{-}55)$$

where $F_i > F_{PL} = F_{cy}(.005)^{1/n}$

and $E_{tan} = E_{sec} = E$

where $F_i \leq F_{PL}$

F_{cy} is the compression yield stress and n is the shape factor determined from the material stress-strain curve. The stress intensity, F_i, depends on the particular mode being considered, as follows:

Panel Bending Moments - In calculating panel being moments from Equations (12-22) and (12-29a), stress intensity is calculated from panel axial compression and shear stresses, f_c and f_s, at the specified load magnitude rather than at failure:

$$f_i = (f_c^2 + 3f_s^2)^{1/2} \tag{12-56}$$

Panel General Instability - Stress intensity for use with Equations (12-29) and (12-30) is a function of combined axial compression, bending, and shear stresses at failure:

$$F_i = [(F_c + F_b)^2 + 3F_s^2]^{1/2} \tag{12-57}$$

Flat Buckling - Stress intensity is a function of the axial compression stress and the maximum shear stress in the flat at failure: For use with Equations (12-31):

$$F_i = [F_c^2 + 3\,(F_{sflat})^2]^{1/2} \tag{12-58}$$

For use with Equations (12-32):

$$F_i = [F_c^2 + 3F_s^2]^{1/2} \tag{12-59}$$

Bead Crippling - Stress intensity for use with Equations (12-33) and (12-34) is a function of the maximum compression stress in the outermost fiber of the bead and the shear stress at failure:

$$F_i = [(F_c + F_b)^2 + 3F_s^2]^{1/2} \tag{12-60}$$

Diagonal Buckling - Stress intensity for use with Equations (12-35) is a function of the axial compression and shear stresses at failure:

$$F_i = (F_c^2 + 3F_s^2)^{1/2} \qquad (12\text{-}61)$$

13.0 PANEL DESIGN STUDIES

The first analysis task, after initial development of OPTRAN code modules for the various panel configurations, was to conduct a series of trade studies to determine the effects of parameter range restrictions, panel configuration, and load configuration and magnitude on panel weight efficiency. The primary purposes of these studies were to establish configuration trends which would influence selection of manufacturing methods, and finally, to select the panel configurations which would be retained for the principal development effort under the contract.

13.1 Initial Trade Studies

The first objective was to study the interaction between panel configuration geometry and panel weight efficiency. The influence of bead depth was of particular interest because it was a primary factor in determining whether manufacturing was to be by brake forming or by stretch forming. The results of these initial trade studies are summarized and presented in this section.

Most of the initial work was done with the Type 1 panel configurations because this was considered at the start of the program to be a principal candidate for final development. The initial trade studies were conducted before the static strength equations were available in their final form, as presented in Section 12. Particularly, the plasticity corrections were generally not included. Therefore, the results presented in this section should be regarded as indicative of trends rather than as absolute values.

Figure 13-1 shows the effects of bead depth, as measured by the included angle, 2α, on panel efficiency. The weight penalty incurred by varying the bead angle from its optimum value is given in percent of the least weight for the optimum panel design having a flat width constrained to 0. All panel designs represented in the figure were optimized for the following combination loading in compression, shear, and bending:

$$N_x = 2000 \text{ lb/in}, \quad N_{xy} = 667 \text{ lb/in}. \quad {}_p = 1.0 \text{ psi}.$$

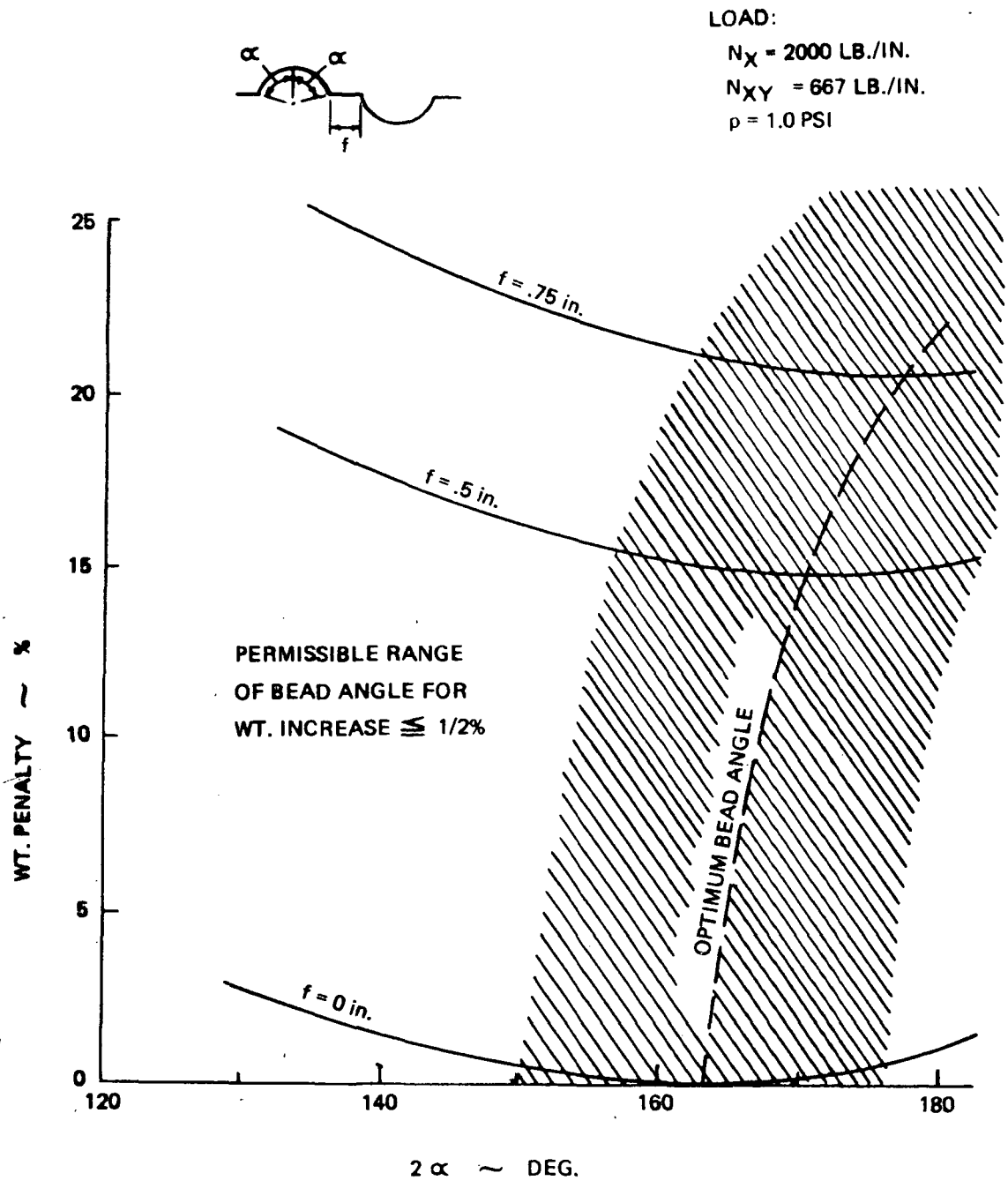

Figure 13-1: WEIGHT PENALTY VS. BEAD ANGLE AND FLAT WIDTH—PANEL TYPE 1

The optimum bead angle is seen to vary with the flat width, from approximately 160 degrees at zero flat width, to approximately 180° at a flat width of .75 inch. The optimum value of the bead angle for variations in flat width is indicated by the dashed curve. The broad, shaded band on either side of the dashed curve indicates the permissible range of bead angles which will increase the weight penalty, for constant flat width, by not more than 1/2% over that incurred with the optimum bead angle. It is apparent that bead angle can be varied at least $\pm 10°$ from the optimum value with less than one half of one percent weight penalty incurred. Thus, panel efficiency is relatively insensitive to bead angle.

It is also apparent from Figure 13-1 that variations in flat width have a pronounced effect on panel efficiency. This effect is a function of load magnitude and is illustrated in Figure 13-2, where weight versus flat width is plotted for several load magnitudes. These plots were obtained using the optimum bead angle, as indicated in Figure 13-1, for each variation in flat width. Note from Figure 13-2 that weight penalties of 5 percent to 10 percent result from a flat width as small as .2 inch.

Figure 13-3 shows the effects of bead angle, 2α, on panel efficiency of the type 2, tubular configuration. The optimum bead angle is seen to be 180° except when the magnitude of the load is such that minimum material gage restrictions control the design. As in the case of the type 1 panel, the type 2 panel efficiency is relatively insensitive to bead angle, except when the design is constrained by minimum material gage, and variations up to 10° from the optimum bead angle can be tolerated with not more than one half percent increase in panel weight. In contrast to the type 1 configuration it has been found that the efficiency of the type 2 panel configuration is relatively insensitive to variations in flat width. Variations in flat width are compensated for by changes in bead radius and thickness, and designs which are constrained to different values of flat width are found to have the same weight as the unconstrained optimum designs.

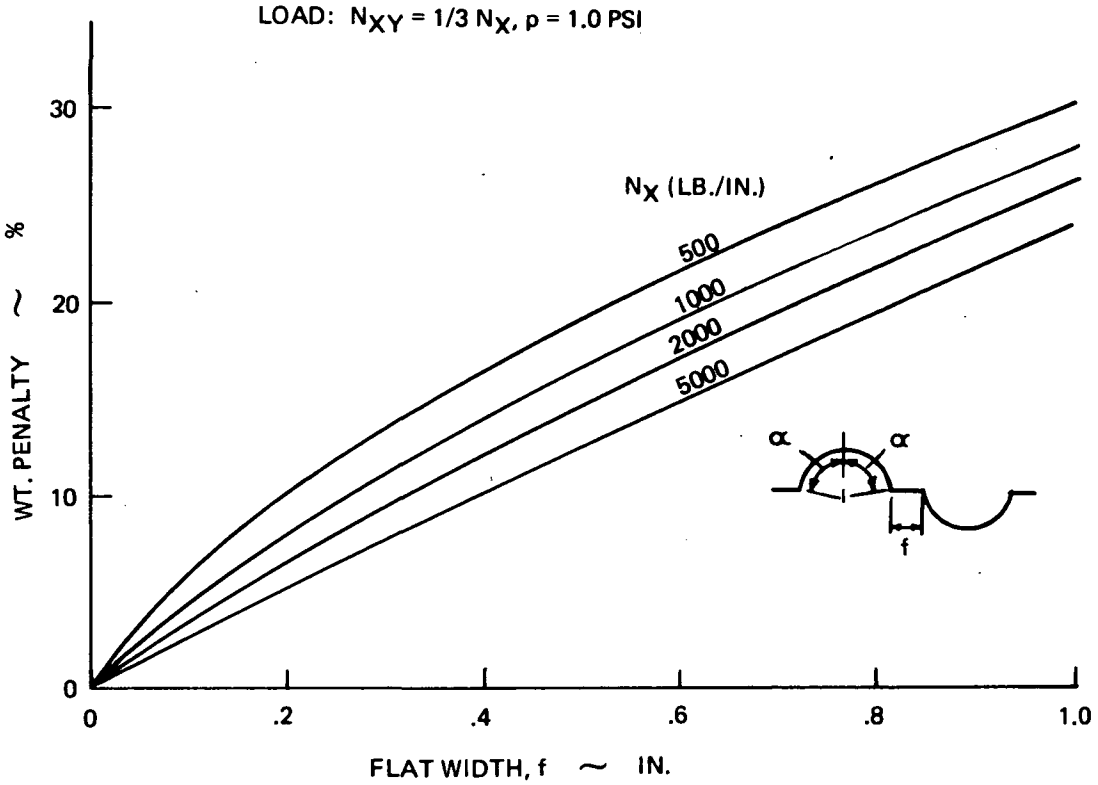

Figure 13-2: WEIGHT PENALTY VS. FLAT WIDTH, VARIOUS LOAD LEVELS–PANEL TYPE 1

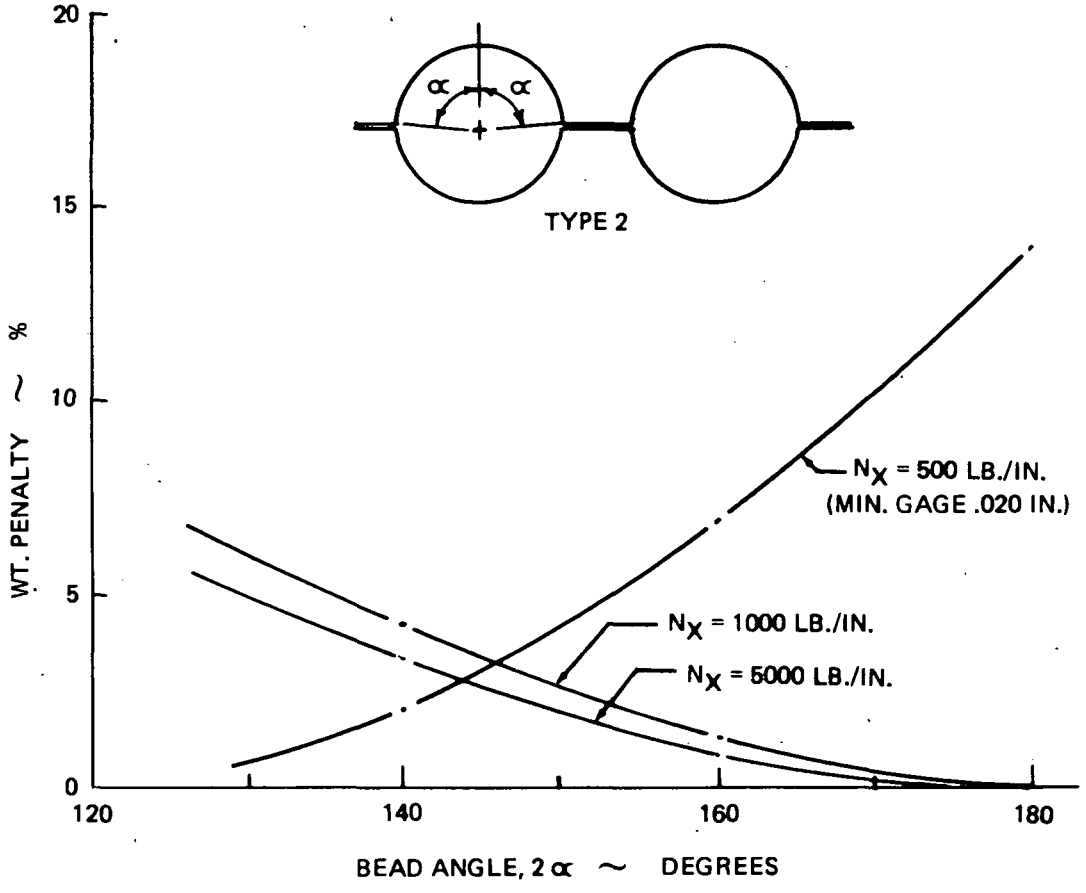

Figure 13-3: WEIGHT PENALTY VS. BEAD ANGLE FOR VARIOUS LOADS–PANEL TYPE 2

Five basic panel configuration types were selected as candidates for the principal development effort. The comparative weights of these configurations versus load are presented in Figure 13-4. The two solid line curves in the figure, for the type 1 configuration with and without flat, are from OPTRAN runs which included plasticity corrections. In all other cases plasticity corrections have not been included. The plasticity corrections had negligible effect on the panel weight curves for the type 1 configurations below the 2000 lb/in load level. Above this load level the effect of the plasticity corrections is to make the type 1 panels appear relatively heavier with respect to the other configurations and direct comparison is not valid.

13.2 Final Design Selections

Four basic design configurations were selected for detailed investigation in this program. These are shown in Figure 13-5. The selection was based on the initial trade study results which appeared in Figure 13-4. Two design load conditions were selected in order to establish the validity of the design and analysis methods over a range of loads representative of a variety of aerospace vehicle structural applications. These load conditions, representing a low load level and a high load level, are identified as load conditions 1 and 2 in Figure 13-5. They are characterized by their principal axial compression components, 600 lb/in and 2000 lb/in, respectively. At the high load level the type 2A configuration is clearly indicated in Figure 13-4 to be superior to all others considered. This was the basis for selecting the 2A-2 design. Although the efficiency of the type 2A configuration is compromised at the lower load level because of minimum gage restrictions, the 2A-1 design was selected to provide a data base for evaluating the configuration over a range of loads. The single sheet configurations were not considered promising because a satisfactory, flight end closure design which could transmit the required shear load was not achieved (See summary document, NASA CR-2514). However, since the type 1A panel is clearly indicated in Figure 13-4 as the most efficient configuration at the low load level, the 1A-1 design was selected anticipating that future development work might solve the end closure problem. The 2-2 design was selected primarily as a backup in case unexpected problems

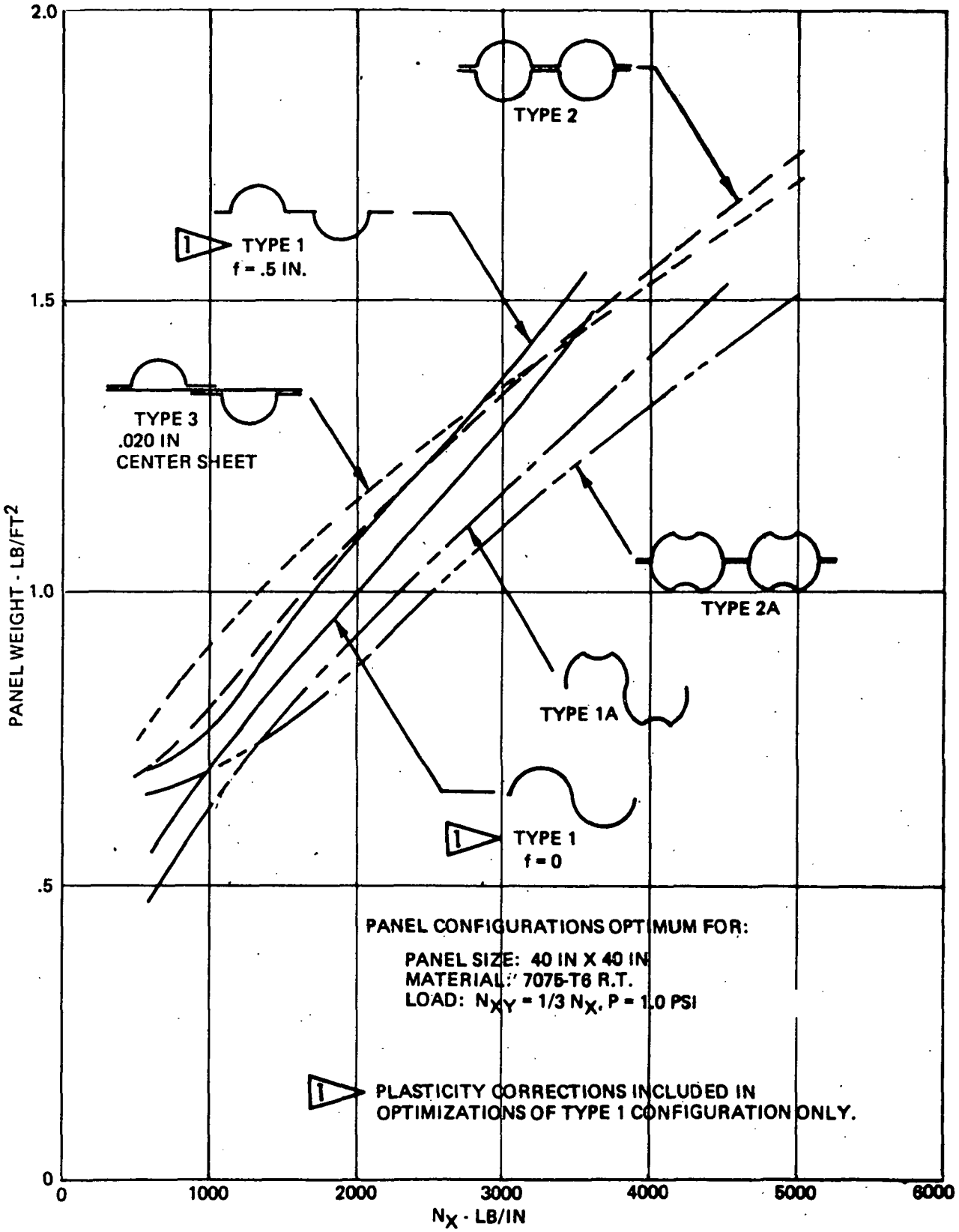

Figure 13-4: COMPARATIVE WEIGHTS OF BEADED AND TUBULAR PANEL CONFIGURATIONS

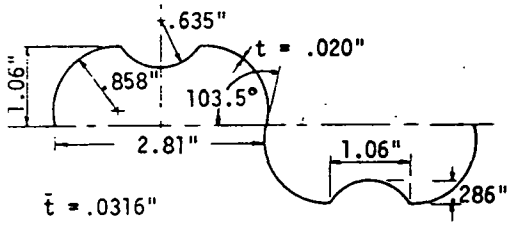

FLUTED SINGLE SHEET (1A-1)

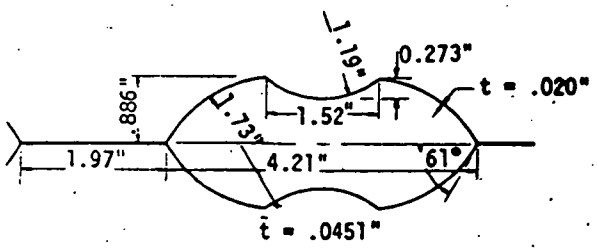

FLUTED TUBE (2A-1)

PANELS OPTIMIZED FOR DESIGN LOAD CONDITION 1:

N_X = 600 LB/IN

N_{XY} = 200 LB/IN

P = 1.0 PSI

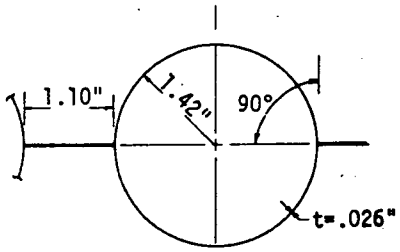

CIRCULAR TUBE (2-2)

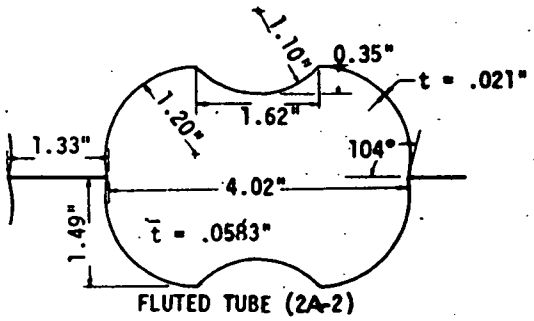

FLUTED TUBE (2A-2)

PANELS OPTIMIZED FOR DESIGN LOAD CONDITION 2:

N_X = 2000 LB/IN

N_{XY} = 400 LB/IN

P = 2.0 PSI

Figure 13-5: OPTIMUM PANEL DESIGNS SELECTED FOR FINAL DEVELOPMENT

should occur in manufacturing or testing the fluted configurations which might compromise their potential efficiencies.

The actual manufactured panel configurations differed slightly from those shown in Figure 13-5 in order to use standard commercially available material thicknesses. Thus, the 2-2 and the 2A-2 designs were reduced in thickness to .025 in. and to 0.20 in., respectively. In the case of the 2-2 design the radius and flat width were reduced proportionately to the thickness reduction, to R = 1.34 in. and f = 1.04 in. For the 2A-2 design, initial end closure development work was already completed using the dimensions indicated in the figure. Therefore, these dimensions were retained to save the cost of remaking the dies.

The predicted strengths of the 2-2 and the 2A-2 panels differ from the design loads indicated in Figure 13-5 because of the thickness reductions. Furthermore, preliminary local buckling test results indicated that an initial assumption that the ridge at the crest of the fluted bead would have a stabilizing effect on bead web failure in bending was an incorrect assumption. Thus, modification to the critical bending stress equations which reduced the critical load for all fluted configurations was made subsequent to the final design selection. These modifications are reflected in the equations given in Section 12 for the fluted configurations. Figure 13-6 shows the panel designs as manufactured, with the revised strength predictions.

Since the original OPTRAN design was changed for the two high load panel designs, a question arose concerning how far off optimum the manufactured test panels might be. This question was answered by re-optimizing these two panel designs for design loads equal to the predicted strength of the manufactured panels. In each case virtually identical panel designs and minimum panel weights were obtained. From these results it was concluded that the manufactured panel designs were, in every practical sense, optimum.

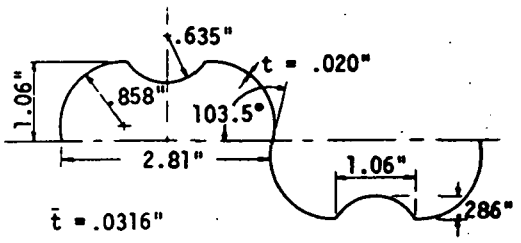

FLUTED SINGLE SHEET (1A-1)

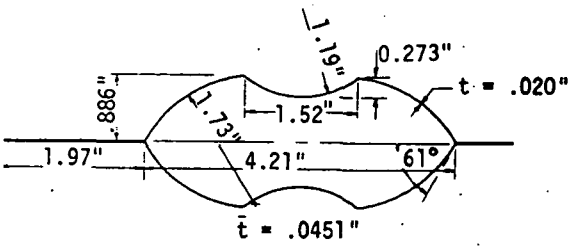

FLUTED TUBE (2A-I)

PREDICTED PANEL STRENGTHS (REVISED)

N_X = 558 LB/IN

N_{XY} = 186 LB/IN

p = 1.0 PSI

N_X = 498 LB/IN

N_{XY} = 166 LB/IN

p = 1.0 PSI

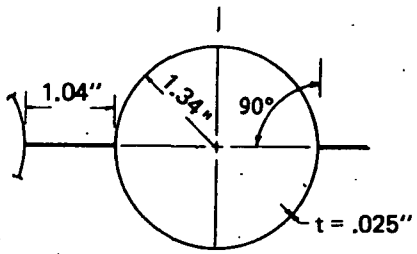

CIRCULAR TUBE (2-2)

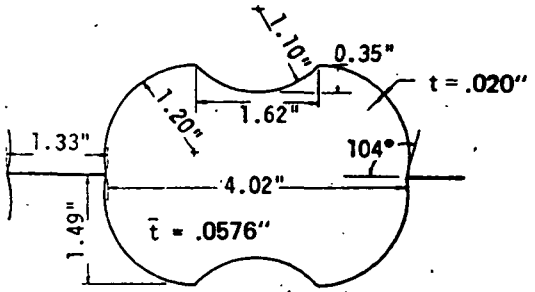

FLUTED TUBE (2A-2)

PREDICTED PANEL STRENGTHS (REVISED)

N_X = 1791 LB/IN

N_{XY} = 358 LB/IN

p = 2.0 PSI

N_X = 1685 LB/IN

N_{XY} = 337 LB/IN

p = 2.0 PSI

Figure 13-6 : OPTIMUM PANEL DESIGNS AS MANUFACTURED WITH REVISED STRENGTH PREDICTIONS

14.0 CORRELATION WITH TEST DATA

Correlation of the analysis with test data consists of two steps. The first step is a preliminary one in which analytical local buckling strengths are compared with local buckling test results, and the static strength equations are modified as necessary to achieve the desired correlation.

Except in cases of pure shear loading critical stresses from local buckling tests are determined from strain gage readings in critical locations and from average material coupon properties. In the case of pure shear loads applied to the local buckling specimens, critical stresses are calculated from the applied load and net section properties. The second step is the final data correlation in which analytically predicted failure loads are compared with test data from the full size, 40-in. x 40-in. panel specimens.

The purpose of final data correlation is to establish the validity of the analysis method for use in designing minimum weight structural panels to withstand specified design loads of compression, shear, and lateral pressure. Test data from the full size, 40-in. x 40-in. panel specimens is compared with the analysis and discussed. Correlations are based on panel loads rather than on stresses. Ten basic load conditions were established for each panel type. Test results consist principally of nondestructive test data obtained using the F/S test technique, described in Reference 14-1, while loading the panels in each of these ten load conditions.

The goal for final data correlation is five percent. Significant differences between analysis and test results greater than this are evaluated to determine if further analysis modifications should be made to attempt to bring the correlation within the five percent goal. This goal is achieved only in the case of the circular tubular panel configuration, type 2. Reasons for not attaining this goal with the other configurations are discussed in presenting the data and in Section 15.0.

Material Properties

Material properties used in the data correlation were obtained from coupon test results. Twelve coupons were obtained from each lot of material used in manufacturing the local buckling and panel specimens. Six of these were tensile specimens and six were compression specimens. Three of each type, tension or compression, were longitudinal and three were transverse with respect to the grain direction in the sheet. Average properties used in the data correlation are given in the following table:

PANEL TYPE	E_c 10^6psi	G 10^6psi	F_{cy} ksi	n
2-2-U-X	10.96	3.97	80.4	24.0
1A-2-U-X	10.66	3.86	81.6	24.1
2A-1-U-X	10.56	3.84	81.7	23.6
2A-2-U-X	10.43	3.81	81.5	22.7
2-2-P-X	11.03	3.94	80.3	22.9
1A-1-P-X	10.58	3.85	81.4	22.9
2A-1-P-X	10.77	3.89	81.3	21.4
2A-2-P-X	10.58	3.85	81.4	22.9

The shear modulus, G, in the table is computed from the average of both tension and compression moduli using Poisson's ratio $\nu = .33$, and n is the exponent used in Equations 12-55. All other values are taken from compression coupon tests only. In the case of panel type 1A-1-P-X the coupons were lost prior to testing, and in the case of panel type 2A-2-P-X the quality of the data was too poor to obtain accurate properties. For these two panel types material properties are average values from all of the other .020-inch material coupons tested.

Panel Dimensions

Measured dimensions of panel cross sections were obtained from local buckling specimens. After testing, the potted ends of the specimen were sawed transversely, to expose the rigidly supported specimen cross section, and photographed with a scale to provide an accurate record of the cross sectional shapes.

Average measured dimensions for the fluted configurations were taken from these photographs and are tabulated below:

Panel Type	t	b	h	b_f	ϕ	h_f	f	R_w	R_f
1A-1	.0201	2.80	1.086	1.046	101.1°	.298	0	.860	.608
2A-1	.0197	4.20	.885	1.51	59.4°	.300	1.98	1.65	1.10
2A-2	.0197	3.97	1.51	1.62	105.0°	.382	1.36	1.20	1.05

Since the cross sections of the full size panels were manufactured with the same dies used to manufacture the local buckling specimens, the above values were considered sufficiently accurate to be used in the final data correlation. In the case of the type 2 panel the local buckling specimens are of a different cross section configuration than the full size panels. Therefore, nominal design values were used in final data correlation of the type 2 panels.

14.1 Correlation of Panel Type 2 Data

14.1.1 Local Buckling Specimen Test Data

Failure stresses from local buckling test data are compared with analytical failure stresses in Figures 14-1 and 14-2. Modifications to the local buckling theory using only the local buckling specimen test results did not achieve satisfactory correlation with panel test results. Therefore, results from local buckling failures of the full size, 40 in. x 40 in. panels are included in addition to the results from the small, uniform section, specimens.

The correlation factors are calculated from the equation,

$$C.F. = \frac{1}{2} \quad R_c + R_b + [(R_c + R_b)^2 + 4\ R_s^{\ 2}]^{1/2} \qquad (14\text{-}1)$$

which is derived from the interaction equation,

$$R_c + R_b + R_s^{\ 2} = 1 \qquad (14\text{-}2)$$

SPECIMEN TYPE	SPECIMEN NO.	LOAD TYPE	FAILURE STRESS – KSI			CORRELATION FACTOR	
			TEST	ORIGINAL ANALYSIS	MODIFIED ANALYSIS	ORIGINAL ANALYSIS	MODIFIED ANALYSIS
UNIFORM SECTION LOCAL BUCKLING SPECIMENS R = 1.20 IN. t = .032 IN.	2-2-U-1	B	$F_B = 78.2$	* $F_B = 77.6$	* $F_B = 77.6$	1.01	1.01
	2-2-U-2	S	$F_S = 37.5$	$F_S = 35.0$	$F_S = 35.0$	1.07	1.07
	2-2-U-3	C	$F_C = 69.2$	* $F_C = 75.4$	* $F_C = 68.8$	.92	1.02
	2-2-U-4	C + S	$F_C = 58.5$ $F_S = 17.8$	* $F_C = 62.2$ $F_S = 19.3$	* $F_C = 59.3$ $F_S = 18.4$	.925	.97
	2-2-U-5	C + B	$F_C = 21.8$ $F_B = 58.8$	* $F_C = 20.4$ $F_B = 54.9$	* $F_C = 19.8$ $F_B = 53.4$	1.07	1.10
40 IN. X 40 IN PANEL SPECIMENS (TESTS TO FAILURE ONLY) R = 1.34 IN. t = .025 IN.	2-2-P-1	C + S	$F_C = 38.2$ $F_S = 13.0$	$F_C = 30.7$ $F_S = 10.9$	$F_C = 36.0$ $F_S = 12.3$	1.24	1.06
	2-2-P-3	S	$F_S = 17.6$	$F_S = 13.6$	$F_S = 17.6$	1.29	1.00

*INELASTIC FAILURE

Figure 14-1 CORRELATION OF LOCAL BUCKLING TEST RESULTS WITH ANALYSIS – PANEL TYPE 2

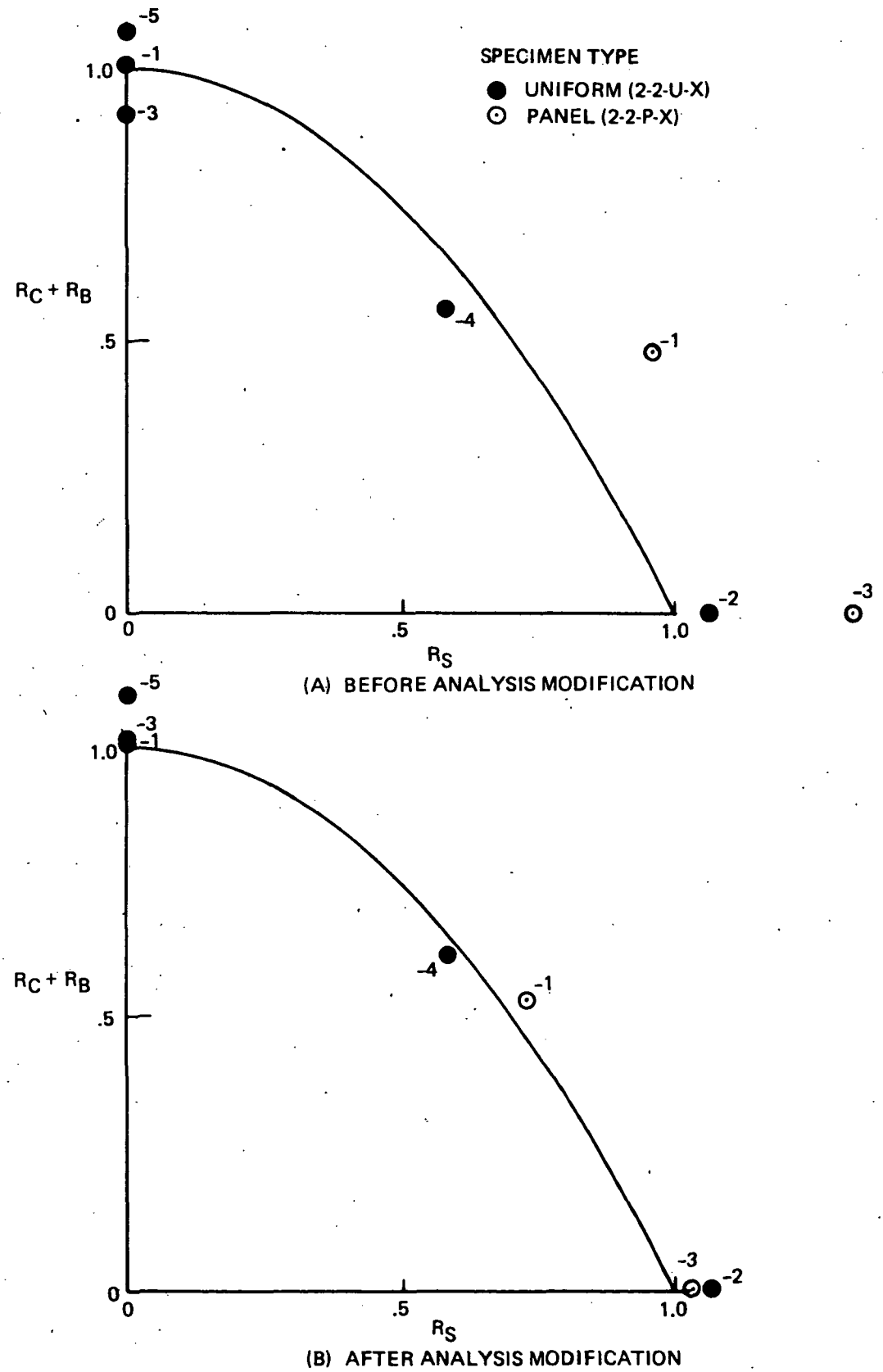

Figure 14-2: LOCAL BUCKLING TEST/ANALYSIS CORRELATION – PANEL TYPE 2 (TEST TO FAILURE, NUMBERS BY DATA POINTS INDICATE SPECIMEN NUMBER)

where R_c, R_b, and R_s are stress ratios of actual stresses at failure to critical stresses in pure compression, bending, and shear respectively. The correlation factor is the ratio of test failure stress to analytical failure stress. Thus, a correlation factor greater than unity indicates that the analysis is conservative.

On the basis of the correlation with the original analysis of Section 12.3, the following modifications to the analyses are made:

(1) The correlations with test of specimens 2-2-U-3 and 2-2-U-4 are brought within desired limits by applying a knockdown factor of .9 to the expression for F_{cc} in Equation (12-33). Thus,

$$F_{cc} = 0.738\ \eta_3\ E\ (t/R)^{1.19} \qquad (14\text{-}3)$$

(2) The correlations with tests of the panel specimens, 2-2-P-1 and 2-2-P-3, are brought within desired limits by changing the expression for the shear buckling coefficient in Equation (12-34) as follows:

$$k_s = 3.3\ Z^{.585} \qquad (14\text{-}4)$$

This change is primarily a change in the length effect which is represented by a series of curves, in the analysis of Reference 12-6, giving k_s as a function of Z for various length ratios (a/b). The original expression for k_s was taken from the curve for $a/b = \infty$. Correlations with the short, local buckling specimens were made using the curve for $a/b = 3$. The change represented by Equation (14-4) approximates a curve which is closer to the latter, thus reducing the length effect for long panels in this application.

The improved correlation obtained with the modified analysis is seen in comparing the last two columns of Figure 14-1. A graphical representation of the local buckling test/analysis correlation before and after analysis modification is seen in Figure 14-2.

14.1.2 Panel Test Data

Three 40 in. x 40 in. panel specimens of the type 2 configuration (2-2-P-1, 2-2-P-2, 2-2-P-3) were each tested in ten different load conditions as follows:

TEST LOAD CONDITION	COMP. VS SHEAR LOAD RATIO		LATERAL PRESSURE p = CONSTANT
	N_x	N_{xy}	(psi)
1	1	0	0
2	0	1	0
3	1	1/5	0
4	1	1/3	0
5	1	0	1.0
6	1	0	2.0
7	0	1	1.0
8	0	1	2.0
9	1	1/5	1.0
10	1	1/5	2.0

Failure loads were predicted for each of the 10 load conditions above using the local buckling analysis, modified as shown in Equations (14-3) and (14-4), and using average material properties from material control coupon tests. These loads are compared with test results in Figure 14-3. Only the major load component, N_x or N_{xy}, is given for each load condition. Test loads are nominal values determined from the applied loads assuming uniform stress distribution with a calculated panel net-to-gross area ratio of .396 (60.4 percent of gross area is edge chord area) and a net panel width of 40 inches. Shear load is assumed to be carried entirely in the net panel.

A graphical representation of the theoretical panel failure load interaction surface with test data is seen in Figure 14-4. The indicated axes, R_c and R_s in the figure are ratios of N_x and N_{xy} at failure to the critical failure loads in compression alone and shear alone. Curves are shown for three different values of pressure. The numbers beside data points indicate test load conditions.

LOAD COND	LOAD TYPE	ULTIMATE LOAD, N_x OR N_{xy} - LB./IN.				CORRELATION FACTOR		
		MODIFIED ANALYSIS	TEST					
			2-2-P-1	-2	-3	2-2-P-1	-2	-3
1 BC	C	† 3098	3000	3180	2940	.97	(1.03)	.95
PI		3098	3080	2880	3000	(.99)	.93	(.97)
2	S	876	870	895	*878	.99	1.02	1.00
3	C+S	2615	2715	3070	2685	1.04	1.17	1.03
4	C+S	1966	*2080	2090	2040	1.06	1.06	1.04
5	C+B	† 2648	3200	2685	2705	1.21	1.01	1.02
6	C+B	† 2300	2750	2425	2210	1.20	1.05	0.96
7	B+S	849	842	885	858	.99	1.04	1.01
8	B+S	823	837	868	818	1.02	1.05	.99
9	C+B+S	2325	2485	2475	2390	1.07	1.06	1.03
**10	C+B+S	2074	2040	2230	2100	.98	1.08	1.01
					AVERAGE	1.053	1.047	1.004

* ACTUAL FAILURE LOADS
**PANEL DESIGN LOAD CONDITION
† INELASTIC FAILURE

ALL FAILURES ARE BEAD CRIPPLING (BC) EXCEPT FOR PANEL INSTABILITY (PI) AS NOTED IN CONDITION 1.

Figure 14-3 FINAL TEST/ANALYSIS CORRELATION SUMMARY–PANEL TYPE 2

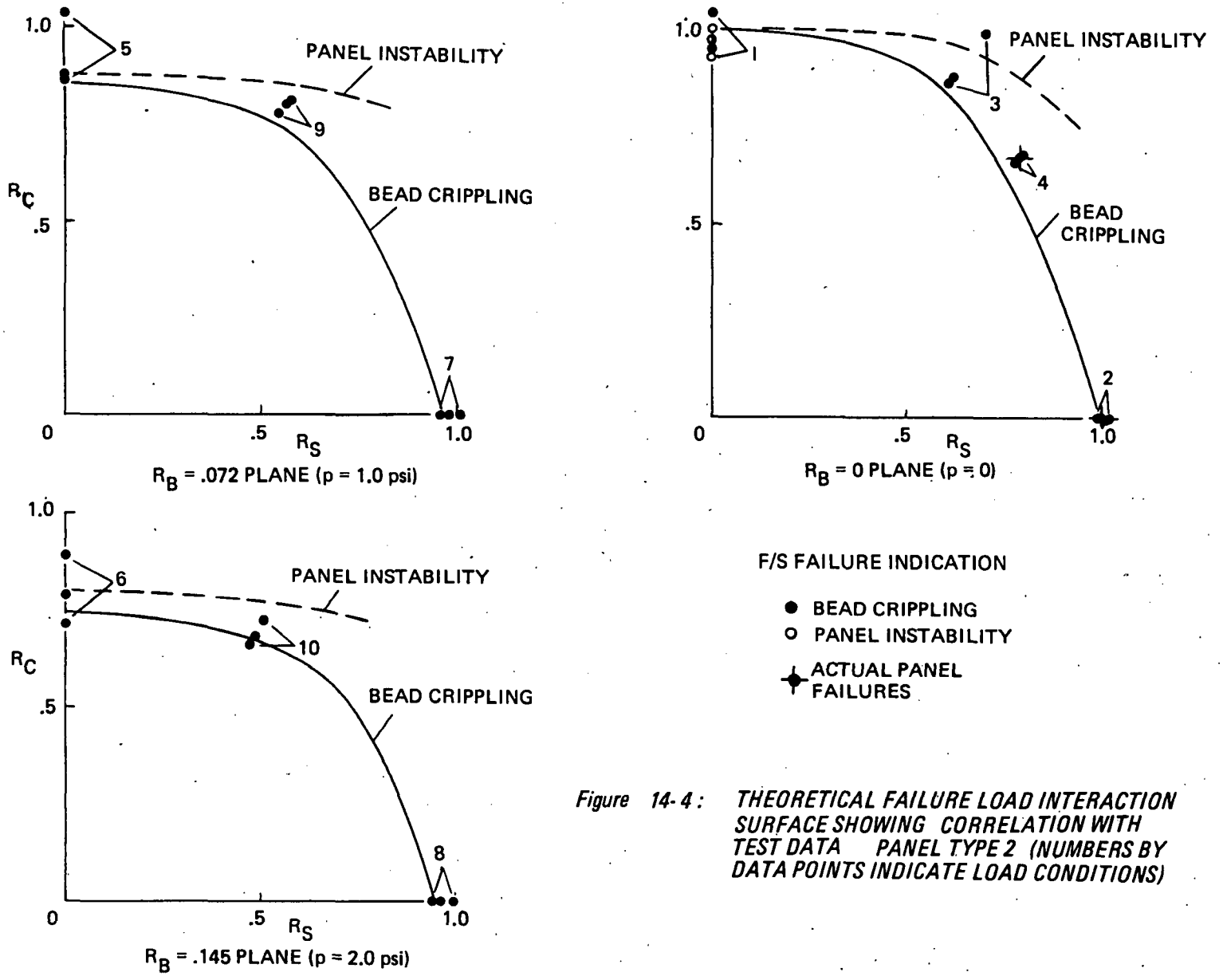

Figure 14-4: THEORETICAL FAILURE LOAD INTERACTION SURFACE SHOWING CORRELATION WITH TEST DATA PANEL TYPE 2 (NUMBERS BY DATA POINTS INDICATE LOAD CONDITIONS)

All test results are F/S failure predictions, except where actual failure loads are indicated for the -1 and the -3 panels. Test failure of the -2 panel was an edge failure which occurred prematurely during an application of load condition 1. Therefore, the actual failure load for this specimen is not valid for use in correlation. The panel instability failure prediction of 93 percent of the analytical value for the -2 panel in load condition 1 (see Figure 14-9) is probably influenced by the same edge defect which caused the premature edge failure and may, therefore, be unrepresentative of the actual panel capability. The predominate failure mode is bead crippling as can be seen from Figure 14-10. Panel instability becomes a factor only under the conditions $R_b = R_s = 0$; and even then, some test results indicate bead crippling.

The analytically predicted stresses at failure in load conditions 5 and 6 are well into the inelastic material range. The F/S failure loads predicted for these conditions required large extrapolations from elastic test data to inelastic failure and are probably less reliable than the test loads predicted for the other load conditions. This probably accounts for the poor correlation of the -1 panel in these load conditions. The correlations are otherwise generally good. The average correlation factor for all three panels is 1.035, which is within the stated accuracy goal of 5 percent. In calculating average correlation factors only the lesser of the two values given for load condition 1 is used. The larger of the two, in parenthesis, is given for comparison only.

Nominal panel test loads were used in making the correlations because they are representative of loads available to the designer. Net panel test loads were also determined using strain gage data from the panel center region to ensure against possible unconservative correlations which would result if actual panel center loads were significantly less than the nominal values. However, panel center loads were found to be slightly higher than the nominal values. Consequently, the correlation factors shown are based on nominal loads.

14.2 Correlation of Panel Type 1A Data

14.2.1 Local Buckling Specimen Test Data

Failure stresses from local buckling test data are compared with analytical failure stresses in Figure 14-5 and 14-6. The correlation factors are calculated in the same way described for panel type 2. Five test data points were obtained from specimen 1A-2-U-5-CBS by using the F/S nondestructive test technique, which worked quite well in predicting diagonal buckling failures. The correlations are quite good and would be considered acceptable without analysis modification except for the one data point representing combined loading of compression, bending, and shear on specimen 1A-2-U-5CBS. This data point suggests the possibility that bending interacts with compression and shear in the diagonal buckling mode. Such interaction is not recognized in the present analysis of this failure mode, and no modification to the analysis was made.

14.2.2 Panel Test Data

Two 40 in. x 40 in. panel specimens of the type 1A configuration (1A-1-P-1, 1A-1-P-2) were each tested in ten different load conditions as follows:

TEST LOAD CONDITION	COMP. VS. SHEAR LOAD RATIO		LATERAL PRESSURE p = CONSTANT
	N_x	N_{xy}	(psi)
1	1	0	0
2	0	1	0
3	1	1/5	0
4	1	1/3	0
5	1	0	0.5
6	1	0	1.0
7	0	1	0.5
8	0	1	1.0
9	1	1/3	0.5
10	1	1/3	1.0

In testing the -1 panel a pronounced nonuniformity in the axial compression was observed which caused the net compression load at the panel center to be approximately 40 percent higher than the nominal applied value. This

SPECIMEN NO.	LOAD TYPE	FAILURE MODE	FAILURE STRESS KSI		CORRELATION FACTOR
			TEST	ORIGINAL ANALYSIS	
*1A-2-U-1	S	WEB CRIPPLING	$F_S = 31.8$	$F_S = 30.2$	1.05
1A-2-U-2	S	DIAGONAL BUCKLING	$F_S = 13.7$	$F_S = 12.6$	1.09
1A-2-U-3	C + B	(LARGE DEFLECTION – NO FAILURE)	–	–	–
1A-2-U-4	C + S	DIAGONAL BUCKLING	$F_C = 19.2$ $F_S = 8.95$	$F_C = 18.5$ $F_S = 8.60$	1.04
1A-2-U-5	C + S	DIAGONAL BUCKLING	$F_C = 19.3$ † $F_S = 9.41$ †	$F_C = 18.0$ $F_S = 8.80$	1.07
1A-2-U-5	C + S	DIAGONAL BUCKLING	$F_C = 8.37$ † $F_S = 11.8$ †	$F_C = 7.90$ $F_S = 11.2$	1.06
1A-2-U-5	C + B + S	DIAGONAL BUCKLING	$F_C = 16.5$ † $F_S = 7.96$ †	$F_C = 18.1$ $F_S = 8.75$	0.91
1A-2-U-5	S	DIAGONAL BUCKLING	$F_S = 14.0$ †	$F_S = 12.6$	1.11
1A-2-U-5	S + B	DIAGONAL BUCKLING	$F_S = 12.9$	$F_S = 12.7$	1.02
1A-2-U-8	B	WEB CRIPPLING	$F_B = 78.4$	** $F_B = 73.8$	1.06
1A-2-U-9	C	DIAGONAL BUCKLING	$F_C = 33.5$	$F_C = 34.6$	.97

* L = 10 IN. ALL OTHER SPECIMENS, L = 30 IN.

** INELASTIC FAILURE

† F/S PROJECTED FAILURE FROM NONDESTRUCTIVE TEST.

Figure 14-5 CORRELATION OF LOCAL BUCKLING TEST RESULTS WITH ANALYSIS – PANEL TYPE 1A

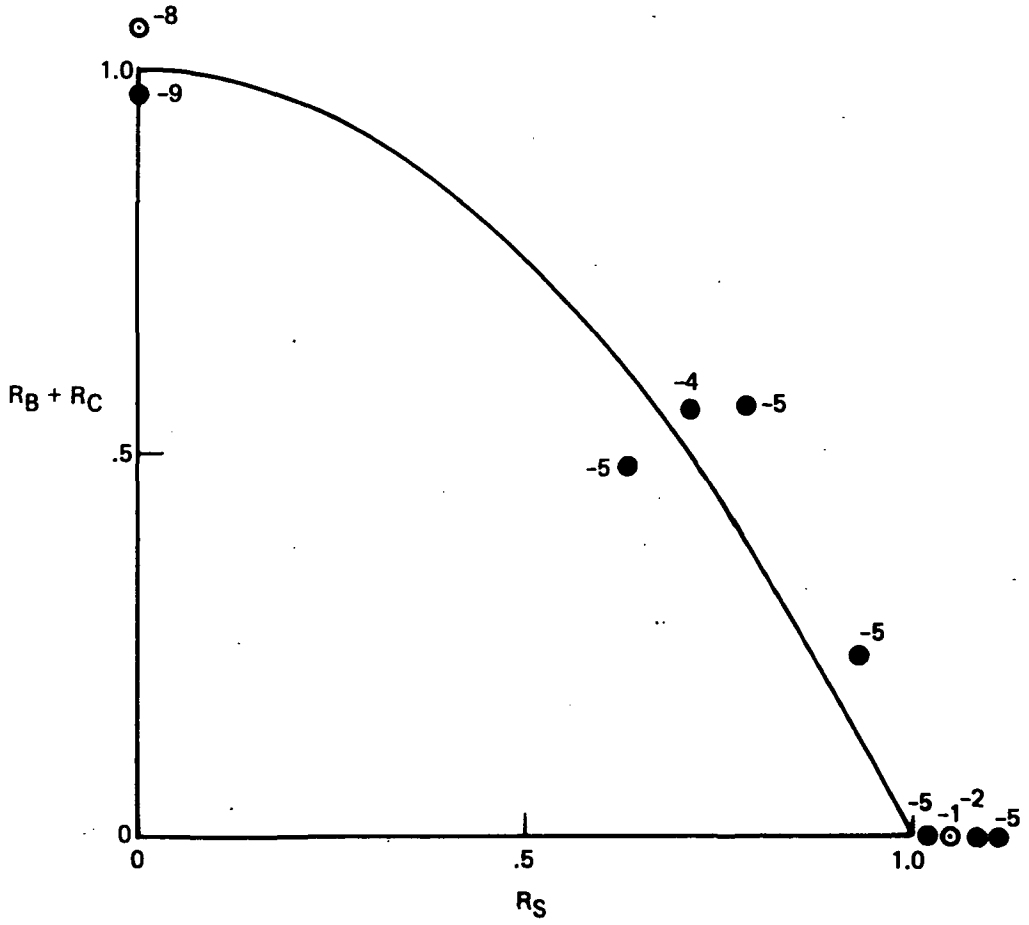

Figure 14-6: LOCAL BUCKLING TEST/ANALYSIS CORRELATION – PANEL TYPE 1A (NUMBERS BY DATA POINTS INDICATE SPECIMEN NUMBER)

peaking of the compression load is caused by a mismatch between the test beam, consisting of the panel specimen with attached chords, and the load application system. This system is better suited to the tubular panels, which constitute the majority of the panels tested, than to the single sheet panels which have a much smaller net-to-gross area ratio. The shear load distribution in the panel was found to be essentially uniform.

The compression load peaking caused the load ratios of N_x to N_{xy} at the panel center to be considerably different from the nominal values given in the above table. On the basis of the -1 panel test results the applied loads were adjusted to give panel center load ratios equal to those given in the table. These adjusted loads were applied in testing the -2 panel.

Analytical failure loads for these panels were computed from average material coupon test properties and average measured dimensions of the cross section as previously described under Section 14.0. A different set of analytical failure loads was calculated for each panel because of the different test load ratios of N_x to N_{xy}. The analytical failure loads are compared with the test results in Figure 14-7. Only the major component, N_x or N_{xy}, is given for each load condition. Test loads are net panel loads determined using strain gage data from the panel center region.

All test results are F/S failure predictions except for the actual failure loads indicated in load condition 10. The diagonal buckling mode was apparently critical in all the test load conditions. This agrees with the analysis except in load conditions 5 and 6 where bead web crippling was predicted to be critical. This is seen more clearly in Figure 14-8 which shows a graphical representation of the theoretical failure load interaction surface with test data.

The average test/analysis correlation of .85 achieved for the type 1A panel indicates the analysis to be unconservative. This appears to be due to a length effect which does not occur in the present diagonal buckling mode analysis. There also appears to be some interaction between bending and compression in the diagonal mode which is not recognized in the present analysis.

LOAD COND.	1A-1-P-1			1A-1-P-2		
	ULTIMATE LOAD N_x OR N_{xy} – LB./IN. ORIGINAL ANALYSIS	TEST	CORRELATION FACTOR	ULTIMATE LOAD N_x OR N_{xy} – LB./IN. ORIGINAL ANALYSIS	TEST	CORRELATION FACTOR
1	1093	880	.80	1093	912	.83
2	249	206	.83	249	225	.90
3	867	790	.91	777	690	.89
4	708	656	.93	588	535	.91
5	† 1070	870	.81	† 1070	880	.82
6	† 938	705	.75	† 938	680	.72
7	249	217	.87	249	218	.88
8	249	212	.85	249	212	.85
9	685	618	.90	584	530	.91
**10	667	*529	.79	548	*487	.89
		Ave.	.844		Ave.	.860

* ACTUAL FAILURE LOADS
** PANEL DESIGN LOAD CONDITION
† INELASTIC BEAD WEB CRIPPLING FAILURE; ALL OTHERS ARE ELASTIC DIAGONAL BUCKLING

Figure 14-7 FINAL TEST/ANALYSIS CORRELATION SUMMARY – PANEL TYPE 1A

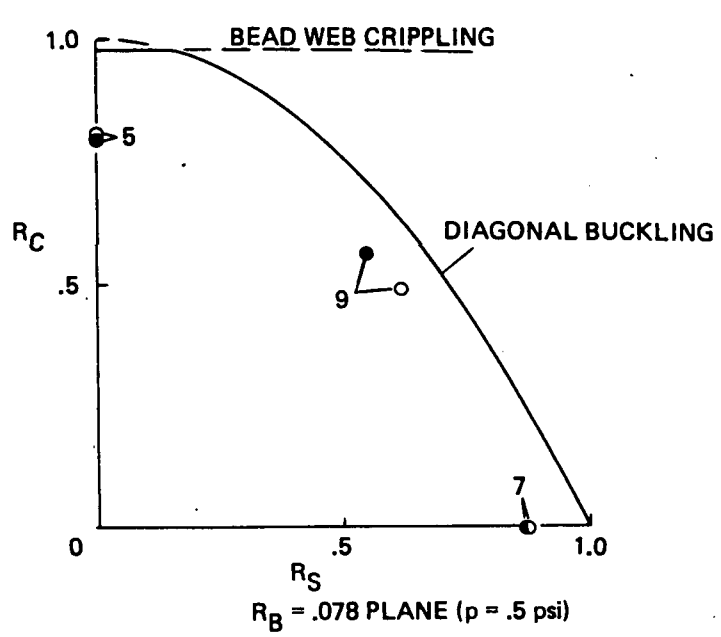

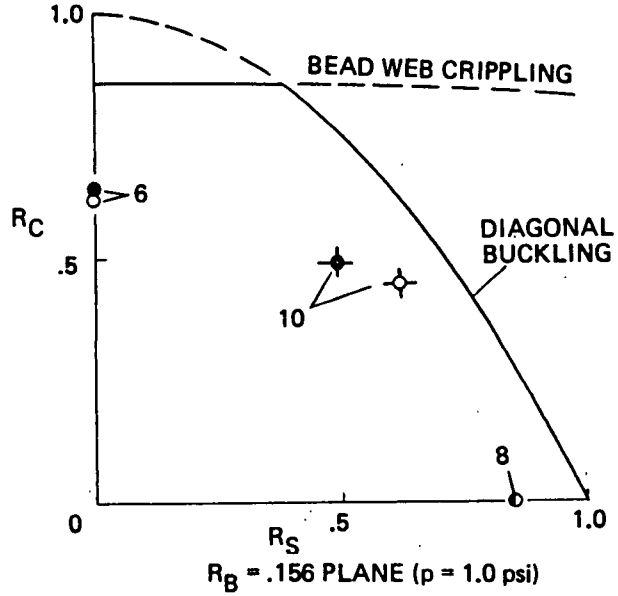

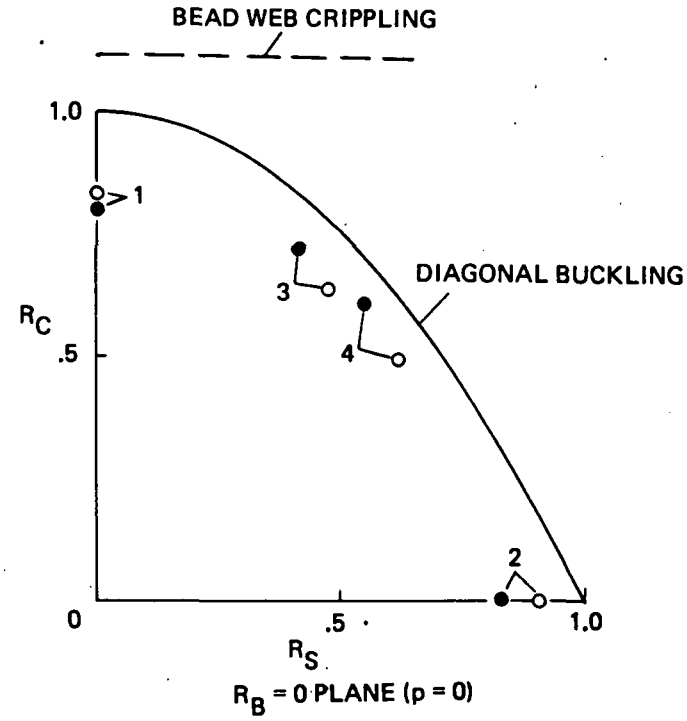

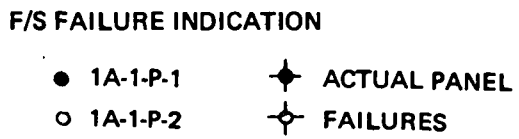

Figure 14-8 : THEORETICAL FAILURE LOAD INTERACTION SURFACE SHOWING CORRELATION WITH TEST DATA PANEL TYPE 1A (NUMBERS BY DATA POINTS INDICATE LOAD CONDITIONS)

14.3 Correlation of Panel Type 2A-1 Data

14.3.1 Local Buckling Specimen Test Data

Failure stresses from local buckling test data are compared with analytical failure stresses in Figure 14-9 and Figure 14-10. The correlation reveals apparent conservatism in most of the results. In the case of flat buckling this is due partly to the separation of the two sheets by the bond layer resulting in increased bending stiffness, and partly to the assumption of simple support at the edges of the flat in the buckling analysis. In spite of the apparent conservatism in the bead crippling combined load and shear analysis there was indication in testing the 30-in. long specimen, 2A-1-U-1-C, that complex modes involving distortion of the cross section and having fairly long wave lengths were occurring. These modes probably could not develop in the shorter specimens, but it was expected that they could occur in the full size panels and considerably reduce the actual buckling stresses. For this reason no analysis modification was attempted on the basis of the local buckling correlations.

14.3.2 Panel Test Data

Only one 40 in. x 40 in. panel of the type 2A-1 configuration was tested. Ten test load conditions were defined as follows:

TEST LOAD CONDITION	COMP. VS. SHEAR LOAD RATIO		LATERAL PRESSURE p = CONSTANT
	N_x	N_{xy}	(psi)
1	1	0	0
2	0	1	0
3	1	1/5	0
4	1	1/3	0
5	1	1/2	0
6	1	0	1.0
7	0	1	1.0
8	0	1	2.0
9	1	1/3	.5
10	1	1/3	1.0

SPECIMEN NO.	LOAD TYPE	FAILURE MODE	FAILURE STRESS KSI		CORRELATION FACTOR
			TEST	ORIGINAL ANALYSIS	
*2A-1-U-1	C	FLAT BUCKLING	$F_C = 24.2$ †	$F_C = 15.6$	1.56
2A-1-U-1	C	WEB CRIPPLING	$F_C = 39.0$	$F_C = 39.4$	.99
2A-1-U-2	C	FLAT BUCKLING	$F_C = 23.4$ †	$F_C = 15.6$	1.51
2A-1-U-2	C	WEB CRIPPLING	$F_C = 37.0$	$F_C = 39.4$	.94
2A-1-U-3	C + B	WEB CRIPPLING	$F_C = 25.5$ $F_S = 44.5$	$F_C = 15.4$ $F_S = 27.4$	1.66
2A-1-U-4	S	WEB CRIPPLING	$F_S = 25.5$	$F_S = 19.5$	1.31
2A-1-U-5	B + S	WEB CRIPPLING	$F_B = 50.5$ $F_S = 17.7$	$F_B = 30.8$ $F_S = 10.8$	1.64
2A-1-U-6	C + S	WEB CRIPPLING	$F_C = 37.3$ $F_S = 11.6$	$F_C = 30.1$ $F_S = 9.35$	1.24
2A-1-U-7	C + B + S	WEB CRIPPLING	$F_C = 25.0$ $F_B = 48.4$ $F_S = 6.12$	$F_C = 14.1$ $F_B = 27.2$ $F_S = 3.44$	1.78
2A-1-U-10	B	WEB CRIPPLING	$F_B = 70.7$	$F_B = 44.1$	1.60

* L = 30 IN. ALL OTHER SPECIMENS, L = 10 IN.

† FLAT BUCKLING STRESSES IDENTIFIED FROM F/S PLOTS.

Figure 14-9 CORRELATION OF LOCAL BUCKLING TEST RESULTS WITH ANALYSIS – PANEL TYPE 2A-1

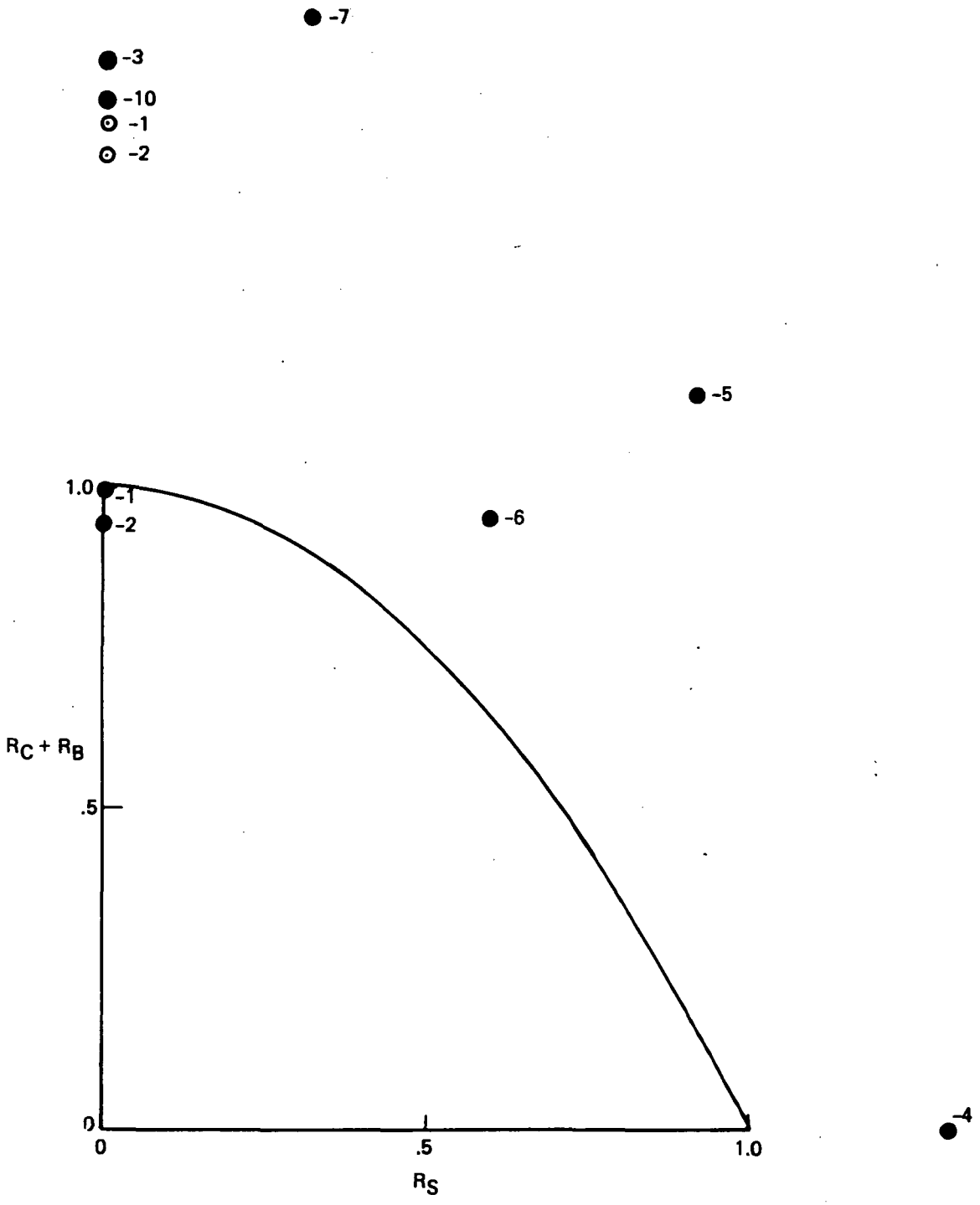

Figure 14-10 LOCAL BUCKLING TEST/ANALYSIS CORRELATION – PANEL TYPE 2A-1 (TEST TO FAILURE, NUMBERS BY DATA POINTS INDICATE SPECIMEN NUMBER)

Force/stiffness plots indicated premature panel instability failure in nearly all load conditions due to pronounced effects of tube distortional modes. In the case of compression and bending loads the distortion observed was flattening of the tubes, while more complex distortions appeared to occur in the presence of shear loads. In pressurizing the panel it appeared that the tubes might collapse before reaching 2 psi; therefore the panel was not tested in load condition 8. The panel was tested to failure in load condition 1. Failure consisted of elastic buckling of the panel with no permanent damage.

After completing the first series of tests the panel was modified by inserting stiffening posts to prevent bead flattening. Six pairs of holes were drilled on the unpressurized side of the panel at the intersections of the bead web and flute. A .10 inch diameter pin, notched at the proper length to maintain the correct internal depth of the tube, was inserted in each hole. The edge of the hole was engaged in the notch and the pin was wedged in place in the hole. The modified panel was designated 2A-1-P-1M and was retested.

The test results are compared with the analysis in Figures 14-11 and 14-12. Average material coupon properties and average measured panel cross section dimensions were used in the analysis as previously described. Test loads are nominal values determined from the applied loads assuming uniform stress distribution with a calculated panel net-to-gross ratio of .303 (69.7 percent of gross area is edge chord area) and a net panel width of 43.3 inches. The trends shown in Figure 14-12 for both test data and theory indicate a shift in failure mode from panel instability to bead web crippling as lateral pressure is increased. However, the test data are in poor agreement with theory.

Significant improvement in the test results was observed with this type of post stiffening, and the panel was eventually tested to failure in the design load condition at 99 percent of the analytical failure load. The panel was still deficient in the presence of large shear components. This is apparently due to the inability of simple post stiffening to provide adequate support against tube distortion other than flattening. It was determined that further testing of the Type 2A-1 panels, even with post type inserts, was not warrented and that further study of the tube distortions could best be accomplished using the Type 2A-2 panels which, because they were not yet fabricated, were amendable to more refined types of inserts.

LOAD COND.	ULTIMATE LOAD N_x OR N_{xy} LB/IN.			CORRELATION FACTOR	
	ORIGINAL ANALYSIS	TEST			
		2A-1-P-1	2A-1-P-1M	2A-1-P-1	2A-1-P-1M
1	700 FB	*530 PI	660 PI	0.76	0.94
2	440 PI	270 PI	338 PI	0.61	0.78
3	682 FB	535 PI	630 PI	0.78	0.92
4	652 FB-PI	470 PI	590 PI	0.72	0.90
5	545 PI	366 PI	420 PI	0.67	0.77
6	483 BWC	458 BWC	485 BWC	0.95	1.00
7	440 PI	335 PI	350 PI	0.74	0.80
8	440 PI	–	–	–	–
9	605 BWC	525 PI-BWC	–	0.87	–
**10	467 BWC	378 PI-BWC	*462 BCW	0.81	0.99
			AVE.	0.768	0.888

*ACTUAL FAILURE LOADS
**DESIGN LOAD CONDITIONS
FB–FLAT BUCKLING, PI–PANEL INSTABILITY, BWC–BEAD WEB CRIPPLING

Figure 14-11 FINAL TEST/ANALYSIS CORRELATION SUMMARY – PANEL TYPE 2A-1

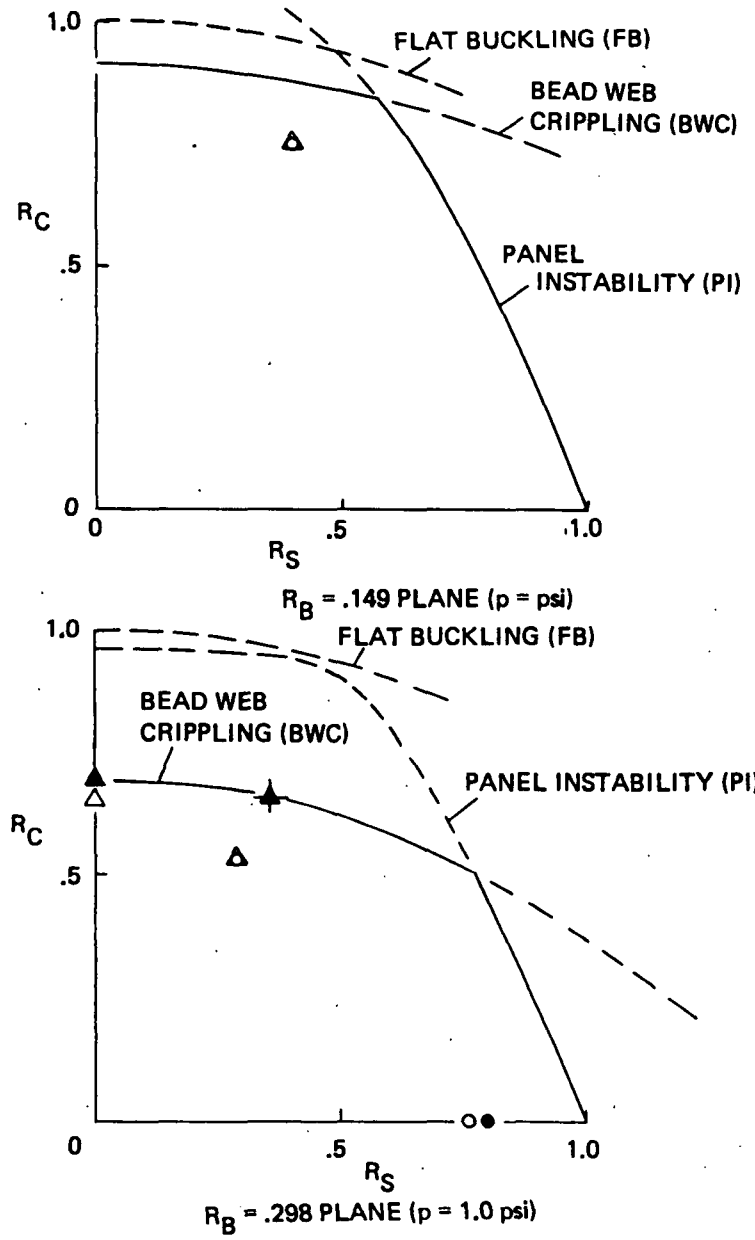

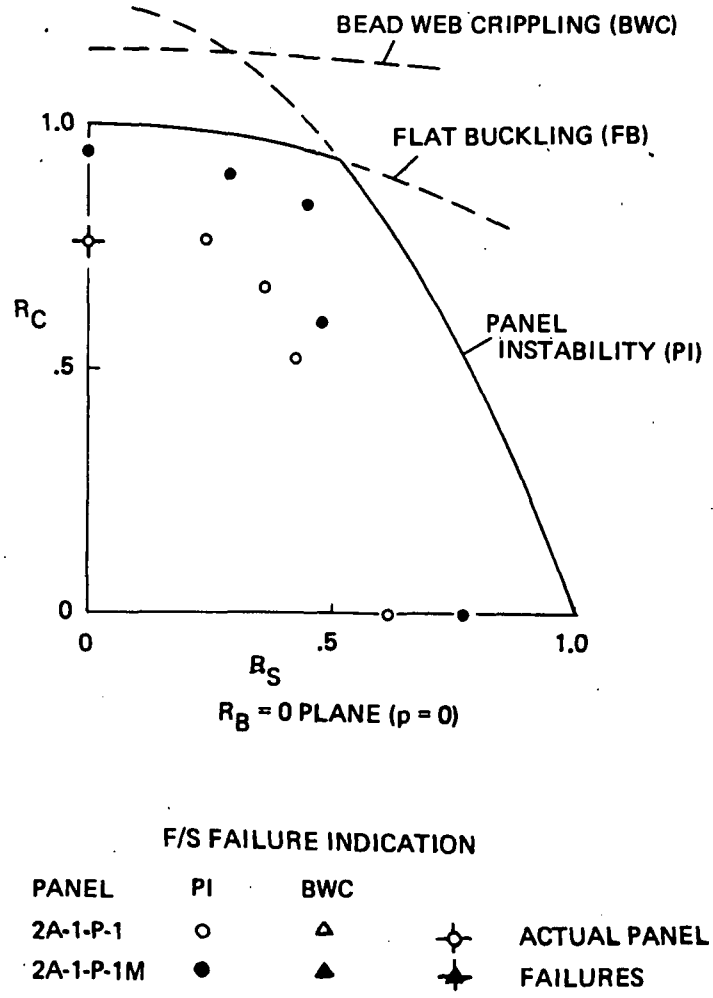

Figure 14-12: THEORETICAL FAILURE LOAD INTERACTION SURFACE SHOWING CORRELATION WITH TEST DATA PANEL TYPE 2A-1

14.4 Correlation of Panel Type 2A-2 Data

14.4.1 Local Buckling Specimen Test Data

Failure stresses from local buckling test data are compared with analytical failure stresses in Figure 14-13 and Figure 14-14. The correlation pattern with the original analysis is similar to that seen in the type 2A-1 specimen tests. The poorer correlation in the case of the two compression specimens is evidence of greater susceptibility of this panel configuration to the cross section distortional mode. This mode was particularly evident from the Moire fringe patterns observed in testing specimen 2A-2-U-2.

On the basis of the correlation with the original analysis of Section 12.3, the following modifications to the bead crippling analysis were made:

(1) The correlations with test specimens 2A-2-U-1 and 2A-2-U-2 are brought within the desired limits by applying a knockdown factor of .8 to the expression for F_{cc} in Equation 12-33. Thus,

$$F_{cc} = .656\ \eta_3\ E\ (t/r)^{1.19} \qquad (14\text{-}5)$$

(2) The correlation with test of specimen 2A-2-U-3, in shear only is brought within desired limits by applying a factor of 1.4 to the expression for F_{cs} in Equation (12-34). Thus,

$$F_{cs} = 1.4\ \eta_2\ G\ k_s\ (t/s_c)^2 \qquad (14\text{-}6)$$

The expressions for k_s and for $\bar{s}$ in Equations (12-34) are unchanged.

(3) To give better correlation with the remainder of the Type 2A-2 local buckling test data, the exponent of the shear term in the interaction equation for bead crippling, Equation (12-36), is changed from 2 to 4.5. Thus, for bead crippling only,

$$R_c + R_s^{4.5} = 1 \qquad (14\text{-}7)$$

SPECIMEN NO.	LOAD TYPE	FAILURE MODE	FAILURE STRESS – KSI			CORRELATION FACTOR	
			TEST	ORIGINAL ANALYSIS	MODIFIED ANALYSIS	ORIGINAL ANALYSIS	MODIFIED ANALYSIS
2A-2-U-1-C	C	WEB CRIPPLING	$F_C = 50.6$	$F_C = 64.3$	$F_C = 51.5$	.79	.98
*2A-2-U-2-C	C	WEB CRIPPLING	$F_C = 53.5$	$F_C = 64.3$	$F_C = 51.5$	.83	1.04
2A-2-U-3-S	S	WEB CRIPPLING	$F_S = 25.5$	$F_S = 18.2$	$F_S = 25.4$	1.40	1.00
2A-2-U-4-CS	C + S	WEB CRIPPLING	$F_C = 37.7$ $F_S = 24.8$	$F_C = 22.3$ $F_S = 14.7$	$F_C = 31.3$ $F_S = 20.6$	1.69	1.20
2A-2-U-6-CB	C + B	WEB CRIPPLING	$F_C = 35.9$ $F_B = 37.3$	$F_C = 32.6$ $F_B = 33.9$	** $F_C = 29.4$ $F_B = 30.5$	1.10	1.22
2A-2-U-7-BS	B + S	WEB CRIPPLING	$F_B = 39.3$ $F_S = 22.1$	$F_B = 25.8$ $F_S = 14.5$	$F_B = 38.1$ $F_S = 21.4$	1.52	1.03
2A-2-U-9-CBS	C + B + S	WEB CRIPPLING	$F_C = 23.2$ $F_B = 36.5$ $F_S = 12.6$	$F_C = 16.0$ $F_B = 25.2$ $F_S = 8.69$	$F_C = 23.1$ $F_B = 36.3$ $F_S = 12.6$	1.45	1.00
2A-2-U-10-B	B	WEB CRIPPLING	$F_B = 68.3$	$F_B = 67.8$	** $F_B = 67.8$	1.01	1.01

*L = 30 IN. ALL OTHER SPECIMENS, L = 10 IN.

** INELASTIC FAILURE

Figure 14-13 CORRELATION OF LOCAL BUCKLING TEST RESULTS WITH ANALYSIS– PANEL TYPE 2A-2

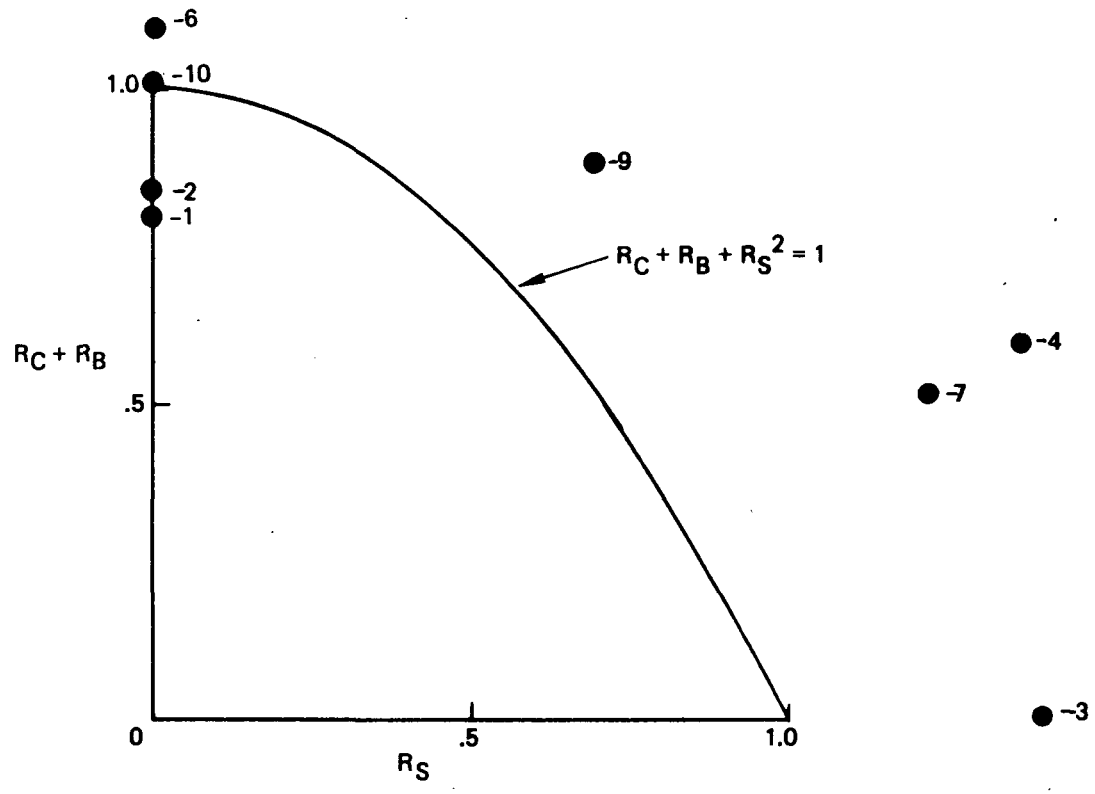

(A) BEFORE ANALYSIS MODIFICATION

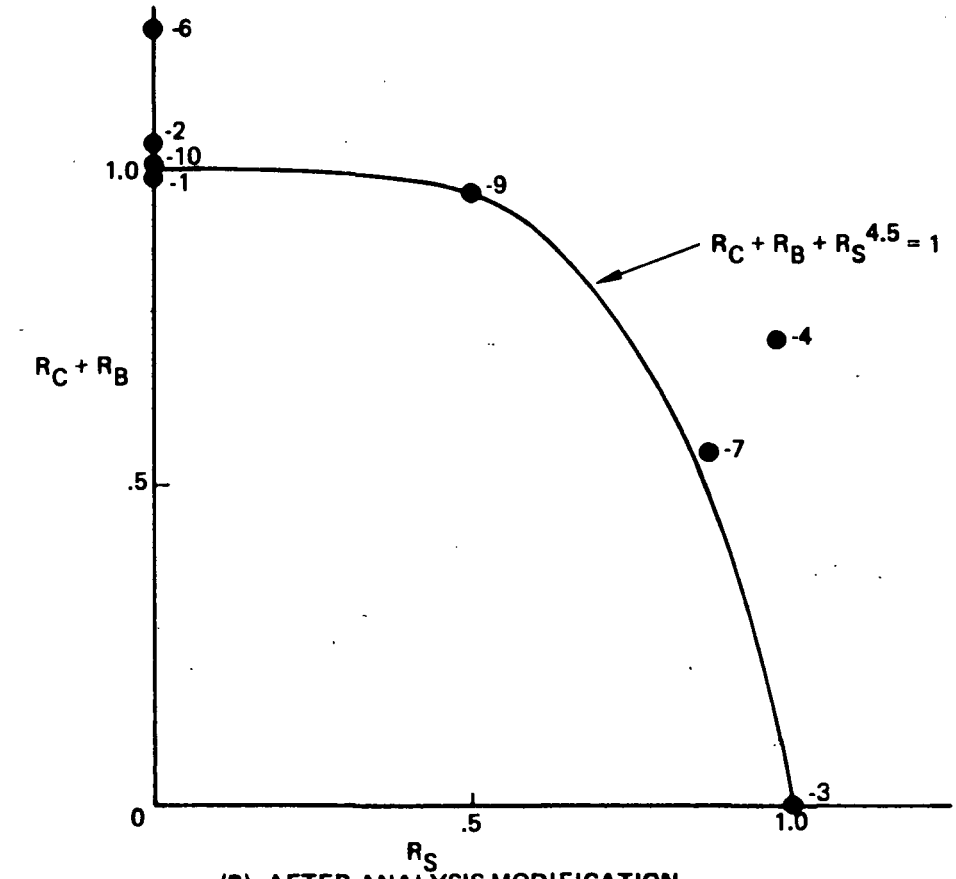

(B) AFTER ANALYSIS MODIFICATION

Figure 14-14: LOCAL BUCKLING TEST/ANALYSIS CORRELATION–PANEL TYPE 2A-2 (TEST TO FAILURE IN BEAD WEB CRIPPLING, NUMBERS BY DATA POINTS INDICATE SPECIMEN NUMBER)

The improved correlation achieved with these modifications to the bead crippling analysis is apparent in Figures 14-13 and 14-14.

No flat buckling test data was obtained from tests of the Type 2A-2 local buckling specimens because they failed in bead web crippling before significant flat buckling modal behavior was observed. However, the flat buckling analysis is known to be conservative for the same reasons given in Section 14.3.1. To obtain more realistic correlation of analysis with panel test data it was decided to modify the flat buckling analysis using the available data from the Type 2A-1 local buckling specimens. Therefore, on the basis of the flat buckling test results for specimens 2A-1-U-1 and 2A-1-U-2 given in Figure 14-9, a factor of 1.5 is applied to the expressions for F_{fc} and F_{fs} in Equations (12-31). Thus,

$$F_{fc} = 1.5\ \pi^2\ \eta_4\ Et^2/[3f^2\ (1-\nu^2)]$$

$$F_{fs} = 8.025\ \pi^2\ \eta_4\ Et^2/[12f^2\ (1-\nu^2)] \qquad (14\text{-}8)$$

14.4.2 Panel Test Data

Three 40 in. x 40 in. panel specimens of the type 2A-2 configuration were tested. the ten test load conditions are identical to those described for panel type 2. Analytical failure loads are compared with test data for these ten load conditions in Figures 14-15 and 14-16. Average material coupon properties and average measured panel cross section dimensions were used in the analysis as previously described. Test loads are nominal values determined from the applied loads assuming uniform stress distribution with a calculated panel net-to-gross area ratio of .350 (65 percent of gross area is edge chord area) and a net panel width of 42.8 inches.

All test data shown in the Figures are from F/S indications of local buckling except where actual panel failures are indicated. The F/S local buckling indications and the test/analysis correlations for specimens 2A-2-P-1M and 2A-2-P-2M are based on the original analysis of Section 12.3. The F/S indications and test/analysis correlations for specimen 2A-2-P-3M are based on the modified analysis described in Section 14.4.1. In Figure 14-16 the test results from specimen 2A-2-P-3M only are compared with the modified theory.

LOAD COND.	ULTIMATE LOAD N_x OR N_{xy}					CORRELATION FACTOR		
	ORIGINAL ANALYSIS	MODIFIED ANALYSIS	TEST					
			† 2A-2-P-1M	†2A-2-P-2M	‡2A-2-P-3M	† 2A-2-P-1M	† 2A-2-P-2M	‡2A-2-P-3M
1	1851 FB	2597 BWC	1260 FB	–	*1790 BWC	0.68	–	0.69
2	730 BWC	1005 BWC	540 PI	*675 BWC	1020 BWC	0.74	0.92	1.01
3	1773 FB	2511 BWC	1230 FB	–	2240 FB	0.69	–	0.89
4	1596 BWC	2128 BWC	1090 PI	1570 BWC	2120 BWC	0.68	0.98	1.00
5	1851 FB	2221 BWC	1250 FB	–	2000 BWC	0.67	–	0.90
6	1851 FB	1926 BWC	1200 FB	–	1800 BWC	0.68	–	0.93
7	704 BWC	987 BWC	580 PI	–	1010 BWC	0.82	–	1.02
8	677 BWC	974 BWC	580 PI	–	1000 BWC	0.86	–	1.03
9	1773 FB	2174 BWC	1250 FB	–	2080 BWC	0.70	–	0.96
**10	1717 BWC	1904 BWC	*1080 BWC	–	1790 BWC	0.63	–	0.94
† F/S RESULTS AND CORRELATIONS BASED ON ORIGINAL ANALYSIS AVG.						0.715	(0.95)	0.937

‡ F/S RESULTS AND CORRELATIONS BASED ON MODIFIED ANALYSIS

*ACTUAL FAILURE LOADS

**DESIGN LOAD CONDITION

FB–FLAT BUCKLING, PI–PANEL INSTABILITY, BWL–BEAD WEB CRIPPLING

Figure 14-15: FINAL TEST/ANALYSIS CORRELATION SUMMARY–PANEL TYPE 2A-2

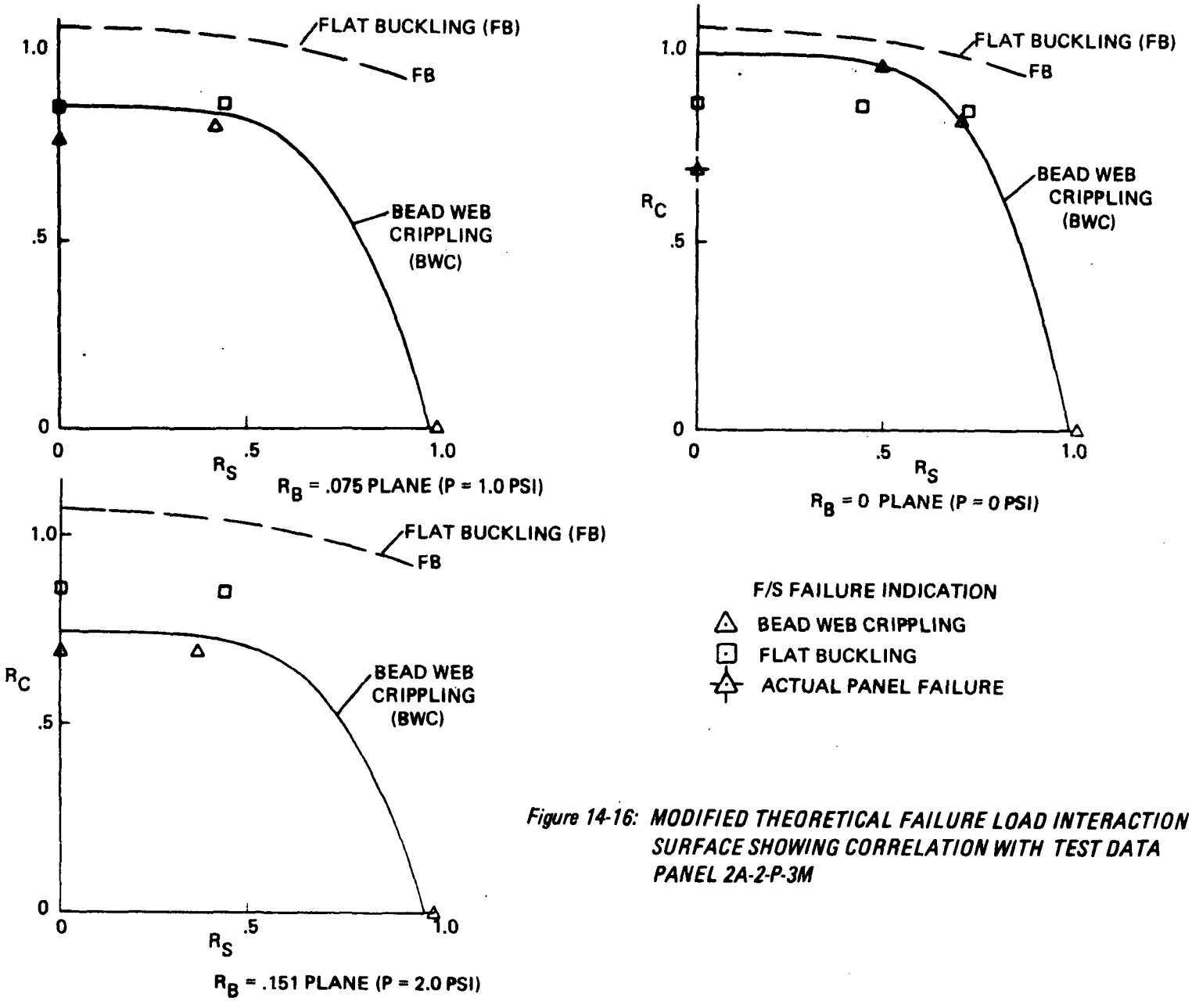

Figure 14-16: MODIFIED THEORETICAL FAILURE LOAD INTERACTION SURFACE SHOWING CORRELATION WITH TEST DATA PANEL 2A-2-P-3M

In testing the first specimen it was immediately apparent that the effect of tube distortional modes was even greater than that observed in the type 2A-1 panel. Therefore, the first specimen was modified by post stiffening similar to that described for the type 2A-1 panel. This specimen was then redesignated 2A-2-P-1M and tested. It was found deficient in all load conditions with premature failure indicated in panel instability or flat buckling at loads averaging 71.5 percent of the analytical failure loads. The specimen finally failed due to bead web crippling in the design load condition at only 63 percent of the analytical failure load. The failure occurred at a location away from the panel center which was not covered by F/S instrumentation. It appeared to be caused by a reduction in curvature of the bead web. This distortion was apparently associated with inadequate transfer of shear load into the panel from the ends.

The second and third specimens were modified by the addition of tube stabilizer inserts during the panel assembly. Details of these modifications are found in Volume 2 of this report which covers fabrication.

The second specimen (2A-2-P-2M) contained modified post type tube stabilizer inserts which were designed to prevent tube flattening and to provide stiffening against other distortional modes that could be identified. Early in testing this specimen an edge defect was discovered which was expected to cause premature edge failure, similar to that which occurred in the case of panel 2-2-P-2, if loaded in axial compression. It was decided to test it to failure in shear rather than risk the edge failure in another load condition. Consequently, test data is only available for two load conditions. These data show a marked improvement with this type of tube stabilization.

The third specimen (2A-2-P-3M) contained a modified arch type of tube stabilizer insert. The insert was designed to maintain the radius of curvature of the tube side walls (the bead web), as well as provide stiffness against the other tube distortional modes. The test results show an improvement in average load carrying capability from 71.5 percent of the analytical failure loads for the first specimen to 93.7 percent for the third specimen.

In some test load conditions shown in Figure 14-16, two different modes of failure are indicated by the F/S test data. Where this occurs both test data points are shown on the figure. Failure modes are identified for all test data points so that they can be compared with the failure loads predicted by the modified theory.

The F/S data for bead web crippling of panel 2A-2-P-3M agree reasonably well with the failure surface predicted by modified theory for most test load conditions. However, the actual failure of the panel by bead web crippling in pure axial compression (load condition 1) occurred at only 69% of the load predicted by the modified theory. This can be explained by the fact that F/S plots of the local buckling kind are extrapolated to a limiting strain line (See Reference 14-1). The limiting strain line is determined from the local buckling analysis as substantiated by local buckling test results. Therefore, F/S indications of panel local buckling behavior are valid only if the local buckling specimen behavior is identical to the panel local buckling behavior. This is apparently not true in the case of the fluted tubular configurations. Complex distortional modes, which are prevented from occurring in the local buckling specimens by their short length and by the stabilizing effect of the potted ends, are only partially restrained by the tube stabilizer inserts in the fuel size panels. Therefore, the correlation indicated in Figure 14-16 between F/S test data and the modified bead web crippling theory is probably not reliable and actual panel failures at substantially smaller load levels might be expected in some load conditions if panels were tested to destruction.

The F/S indications of flat buckling in Figure 14-16 are premature compared to the modified flat buckling theory. This fact indicates that stresses in the flats are higher than they should be according to the panel stress analysis. This phenomenon is due to inadequate load transfer from the panel ends into the tubes, which in turn can be attributed to two causes. First, the transition section at the panel ends was too short. Second, the distortional flexibility of the fluted tube cross section apparently prevents the tubes from carrying their allotted portion of the panel loads. Because of this distortional flexibility, adequate correlation can not be obtained by simple modification of the flat buckling coefficient.

15.0 RESULTS AND CONCLUSIONS

Circular Tube Panel

A satisfactory design and analysis procedure has been established for the circular arc, tubular panel configuration. The final correlation of analysis with test data is good. The average correlation factor for the thirty test points, as well as the majority of the individual values, are within the stated goal of 5%. Therefore, it is recommended that the static strength equations for the type 2 panel configuration, as presented in Section 12 and as modified in Section 14.1 be adopted for design purposes.

A typical set of optimum design curves for circular tubular panels is given in Figure 15-1. These curves were generated using OPTRAN with the modified equations as recommended above, and with nominal design allowable material properties for 7075-T6 aluminum at 70°F. The curves represent a single load configuration of axial compression, shear, and lateral pressure. Similar curves can be generated for other load configurations as required.

The curves in Figure 15-1 also represent a fixed bead angle, $2\alpha = 180$ degrees, and a constant ratio of flat width to bead radius, $f/R = .75$. As discussed in Section 13.1, the 180 degree bead angle is optimum for panels which are not constrained by minimum material gage. Also, because panel efficiency is insensitive to changes in flat width, the ratio f/R can be varied considerably with no measurable change in panel weight for a given length of panel and load magnitude. Therefore, it is possible to generate similar design curves for other ratios of f/R as necessary to satisfy different geometric contraints.

The designs represented by the curves of Figure 15-1 are all geometrically similar in cross section, except for the relative sheet thicknesses. Therefore, the basic panel weight in pounds per square foot is a function of the thickness only, and is easily obtained for any panel size and load from the formula given in the figure. The weight given by the formula is the nominal weight for the uniform section of the panel and does not include the weight penalty for end closures and edge reinforcing. The type 2 panel specimens

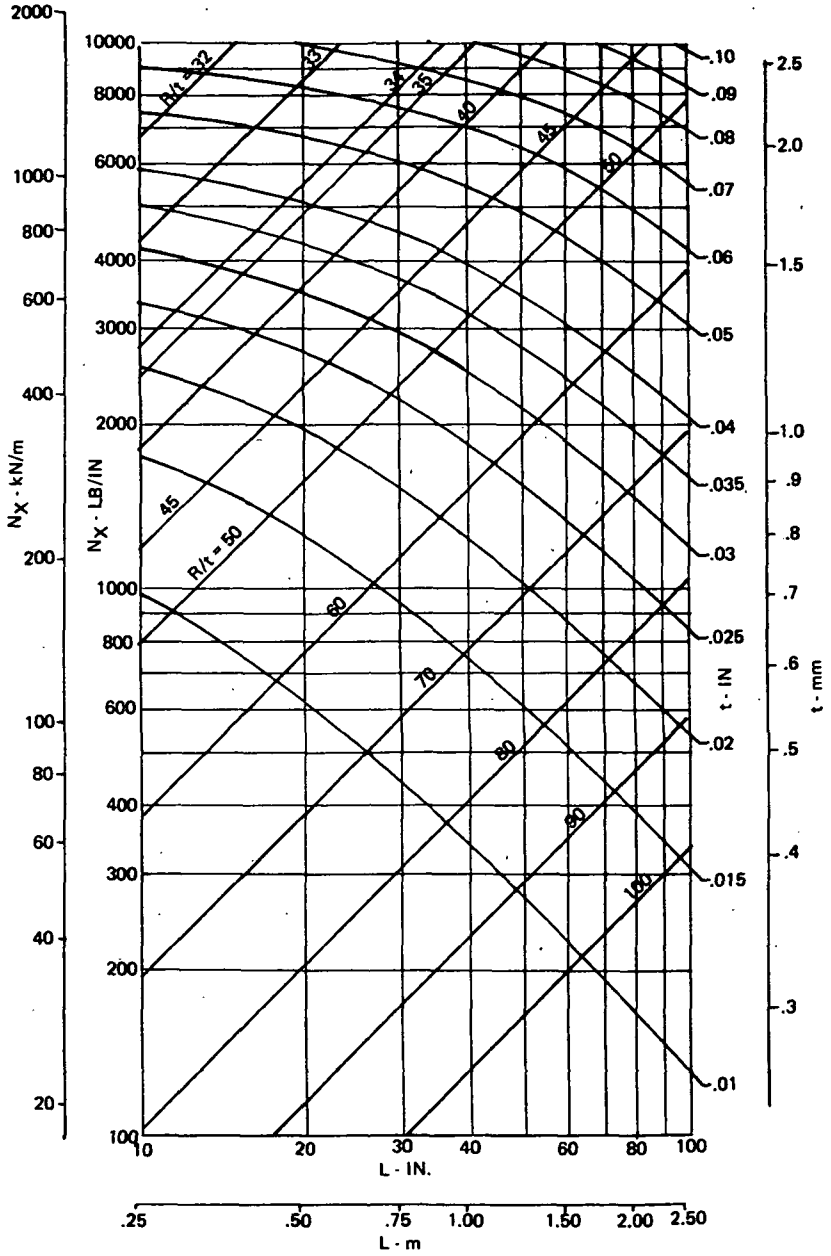

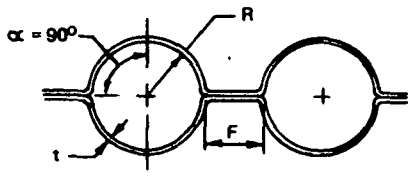

ALUMINUM 7075-T6 70°F

$E = 10.3 \times 10^6$ PSI

$F_{CY} = 68.0$ KSI

$N_{XY} = N_x/5$

$\rho L = .05\ N_X$

$F = .75\ R$

PANEL WEIGHT:
Wt. ($LB./FT^2$) = 41.3t (IN.)

Figure 15-1: TUBULAR PANEL DESIGN DATA

manufactured and tested in this program were weighed and compared with the nominal panel weight. The average joint weight penalty for the 3 panel specimens was 18 percent. This included end closures and edge doublers but not fasteners. It is expected that the joint weight penalty of 18 percent will remain fairly constant regardless of panel size and loading. However, this should be verified when experience over a wider range of panel designs becomes available. One way of reducing the joint weight penalty drastically is to make longer panels with continuous uniform section over intermediate supports. The intermediate supports reduce the effective panel length, L, for design purposes to a fraction of the actual panel length. Thus, effectively two or more panels of length L are obtained, but with the end closure weight of only one.

Fluted Panels

The results of the test/analysis data correlation appearing in Section 14 indicate that a satisfactory design and analysis procedure has not yet been achieved for the fluted panel configurations. The local buckling test results have indicated the analysis to be generally conservative, while the full size panel test results have indicated that the analysis is unconservative. This apparent contradiction is caused by the lack of a satisfactory analysis for the longer wavelength modes, i.e. the diagonal buckling and tube distortional modes, which become dominant in the full size panels.

Before recommending further analysis effort for the fluted panel configurations, relative panel efficiencies need to be reviewed. The fluted tubular and circular tubular panel weights are compared in the following table:

PANEL NO.		TYPE	DESIGN WT.	ACTUAL WT.	WEIGHT PENALTY
2-2-P-1 2-2-P-2 2-2-P-3	(AVE.)	CIRCULAR TUBE	12.6 LB	14.9 LB	18%
2A-2-P-2M		FLUTED TUBE	10.4 LB	14.0 LB	35%
2A-2-P-3M		FLUTED TUBE	10.4 LB	15.4 LB	48%

"Page missing from available version"

REFERENCES

1. Shideler, John L. and Jackson, L. Robert, "Fuselage and Tank Structures for Hypersonic Aircraft," Conference on Hypersonic Aircraft Technology, Ames Research Center, Moffett Field, CA, NASA SP-148, May 1967.

2. Anderson, Melvin S., Robinson, James C., and Klich, George F., "Analysis of Wing Structures for Hypersonic Aircraft," Conference on Hypersonic Aircraft Technology, Ames Research Center, Moffett Field, CA, NASA SP-148, May 1967.

3. Plank, P. P., Sakata, I. F., Davis, G. W., and Richie, C. C., "Hypersonic Cruise Vehicle Wing Structure Evaluation," NASA CR-1568, May 1970.

4. Card, M. F., Davis, J. G., and Shideler, J. L., "Advanced Design Concepts for Shuttle Airframe Structures," NASA Space Shuttle Technology Conference, San Antonio, TX, April 12-14, 1972, NASA TM X-2570, July 1972.

5. Shideler, John L., Anderson, Melvin S., and Jackson, L. Robert, "Optimum Mass-Strength Analysis for Orthotropic Ring-Stiffened Cylinders Under Axis Compression," NASA TN D-6772, July 1972.

6. Musgrove, M. D., Greene, B. E., Shideler, J. L., and Bohon, H. L., "Advanced Beaded and Tubular Structural Panels," J. of Aircraft, Vol. II No. 2, February 1974.

7. Laakso, John R., "Design Synthesis of a Boron/Epoxy Reinforced Metal Shear Web," AIAA/ASME/SAE 13th Structures, Structural Dynamics, and Material Conference, San Antonio, TX, April 10-12, 1972.

8. Jones, Robert E., Greene, Bruce E., "The Force/Stiffness Technique For Nondestructive Buckling Testing," AIAA/ASME/SAE 15th Structures, Structural Dynamics, and Materials Conference, Las Vegas, Nevada, April 17-19, 1974.

REFERENCES (Continued)

11-1 Hague, D. S. and Glatt, C. R., "An Introduction to Multivariable Search Techniques for Parameter Optimization (and Program AESOP)," NASA CR-73200, The Boeing Company, April 1968.

11-2 J. H. Laakso, "Design Synthesis of a Boron/Epoxy Reinforced Metal Shear Web," AIAA/ASME/SAE 13th Structures, Structural Dynamics and Materials Conference, San Antonio, Texas, April 10-12, 1972.

12-1 Timoshenko, S. P. and Gere, J. M., "Theory of Elastic Stability," Second Edition, McGraw-Hill Book Co., 1961.

12-2 Roark, Raymond J., "Formulas for Stress and Strain," Third ed., McGraw-Hill Book Company, Inc., 1954.

12-3 Lekhnitski, S. G., "Anisotropic Plates," Contributions to the Metallurgy of Steel--No. 50, American Iron and Steel Institute, June 1956.

12-4 Nadai, A., "Theory of Flow and Fracture of Solids," Vol. I, Second ed., McGraw-Hill Book Company, Inc., 1950.

12-5 "Buckling of Thin-Walled Circular Cylinders," NASA SP-8007, NASA Space Vehicle Design Criteria (Structures), August 1968.

12-6 Gerard, George and Becker, Herbert, "Handbook of Structural Stability," Part III--Buckling of Curved Plates and Shells, NASA TN 3783, 1957.

12-7 Bleich, F., "Buckling Strength of Metal Structure," McGraw-Hill Book Company, Inc., 1952.

12-8 Plank, P. P., etal, "Hypersonic Cruise Vehicle Wing Structure Evaluation," Lockheed Missiles and Space Co., NASA CR-66897-2, February 1970.

14-1 Jones, Robert E., Greene, Bruce E., "The Force/Stiffness Technique for Nondestructive Buckling Testing," AIAA/ASME/SAE 15th Structures, Structural Dynamics, and Materials Conference, Las Vagas, Nevada, April 17-19, 1974.

NASA CR-132460

DISTRIBUTION LIST
NAS1-10749

	No. Copies
NASA Langley Research Center	
Hampton, VA 23665	
Attn: Report & Manuscript Control Office, Mail Stop 180A	1
Raymond L. Zavasky, Mail Stop 115	1
Technology Utilization Office, Mail Stop 139A	1
Roger A. Anderson, Mail Stop 188	1
Robert W. Leonard, Mail Stop 188	1
Michael F. Card, Mail Stop 190	1
Dr. Martin M. Mikulas, Jr., Mail Stop 190	1
Dr. Paul A. Cooper, Mail Stop 208	1
Dr. Melvin S. Anderson, Mail Stop 190	1
Dr. Jerry G. Williams, Mail Stop 245	1
James C. Robinson, Mail Stop 208	1
Herman L. Bohon, Mail Stop 208	1
Dr. Sidney C. Dixon, Mail Stop 208	1
Harvey G. McComb, Jr., Mail Stop 362	1
James P. Peterson, Mail Stop 245	1
H. Neale Kelly, Mail Stop 208	1
L. Robert Jackson, Mail Stop 160B	1
John L. Shideler, Mail Stop 208	15
NASA Ames Research Center	
Moffett Field, CA 94035	
Attn: Library, Mail Stop 202-3	1
NASA Flight Research Center	
P. O. Box 273	
Edwards, CA 93523	
Attn: Library	1
Roger A. Fields	1
NASA Goddard Space Flight Center	
Greenbelt, MD 20771	
Attn: Library	1
NASA Lyndon B. Johnson Space Center	
2101 Webster Seabrook Road	
Houston, TX 77058	
Attn: Library, Code JM6	1
Jet Propulsion Laboratory	
4800 Oak Grove Drive	
Pasadena, CA 91103	
Attn: Library, Mail 111-113	1
NASA Lewis Research Center	
21000 Brookpark Road	
Cleveland, OH 44135	
Attn: Library, Mail Stop 60-3	1

NASA CR-132460

DISTRIBUTION LIST
NAS1-10749

	No. Copies
NASA John F. Kennedy Space Center Kennedy Space Center, FL 32899 Attn: Library, IS-DOC-1L	1
NASA Marshall Space Flight Center Huntsville, AL 35812	
Attn: Library	1
William A. Wilson, S&E-PE-M	1
National Aeronautics & Space Administration Washington, DC 20546	
Attn: KSS-10/Library	1
RW/NASA Headquarters	1
McDonnell Douglas Corporation Post Office Box 516 St. Louis, MO 63166 Attn: L. C. Koch, M.S. 152	1
AVCO Corporation Aerostructures Division Nashville, TN 37202	1
Bell Aerosystems Company Box 1 Buffalo, NY 14205	1
Bell Helicopter Company P. O. Box 482 Fort Worth, TX 76101	1
General Dynamics Corporation P. O. Box 748 Fort Worth, TX 86101	1
General Dynamics Corporation Convair Division P. O. Box 1128 San Diego, CA 92112	1
Grumman Aerospace Corporation South Oyster Bay Road Bethpage, Long Island, NY 11714	1
Republic Aviation Corporation Farmingdale, NY 11735	1
Lockheed Aircraft Corporation P. O. Box 504 Sunnyvale, CA 94086	1

NASA CR-132460

DISTRIBUTION LIST
NAS1-10749

	No. Copies
Lockheed Aircraft Corporation 2555 North Hollywood Boulevard Burbank, CA 91504	1
Lockheed Aircraft Corporation Lockheed-Georgia Company 86 South Cobb Drive Marietta, GA 30060	1
LTV Aerospace Corporation Grand Prairie, TX 75050	1
McDonnell Douglas Corporation 3855 Lakewood Boulevard Long Beach, CA 90801	1
McDonnell Douglas Corporation 5301 Bolsa Avenue Huntington Beach, CA 92647	1
McDonnell Douglas Corporation P. O. Box 516 St. Louis, MO 63166	2
Martin Marietta Corporation The Martin Company Post Office Box 179 Denver, CO 80201	1
Rockwell International Corporation Los Angeles Aircraft Division International Airport Los Angeles, CA 90009	1
Rockwell International Corporation 12214 Lakewood Boulevard Downey, CA 90241	1
United Aircraft Corporation Sikorsky Helicopter Stratford, CT 06602	1
Kaman Corporation Old Windsor Road Bloomfield, CT 06002	1
Northrop Corporation 1001 E. Broadway Hawthorne, CA 90250	1

NASA CR-132460

DISTRIBUTION LIST
NAS1-10749

	No. Copies
General Electric Company Valley Forge, PA 19481	1
Air Force Flight Dynamics Laboratory Wright-Patterson Air Force Base, OH 45433	1
Rohr Corporation P. O. Box 878 Chula Vista, CA 92010	1
Rohr Corporation 620 East 111th Place Los Angeles, CA 90059	1
Rohr Corporation P. O. Box 643 Riverside, CA 92502	1
NASA Scientific & Technical Information Facility P. O. Box 33 College Park, MD 20740	29 plus reproducible